Retention of ^{10}Be, ^{137}Cs and ^{210}Pb_xs in soils: Impact of physico-chemical characteristics

Félix de Tombeur, Sophie Cornu, Didier Bourlès, Adrien Duvivier, Julie Pupier, Michel Brossard, O. Evrard

Retention of ^{10}Be, ^{137}Cs and $^{210}Pb_{xs}$ in soils: impact of physico-chemical characteristics

de Tombeur, Felix[1, 2], Cornu, Sophie[1,*], Bourlès, Didier[1], Duvivier, Adrien[1], Pupier, Julie[1], ASTER Team[1,**], Brossard, Michel[3], Evrard, Olivier[4]

[1] Aix-Marseille Université, CNRS, Collège de France, IRD, INRA, CEREGE, 13545 Aix en Provence, France
[2] TERRA Teaching and Research Centre, Gembloux Agro-Bio Tech (GxABT), University of Liège, 5030 Gembloux, Belgium
[3] IRD, UMR 210 Eco&Sols (Cirad, INRA, IRD, Montpellier SupAgro), BP 90165, 97323 Guyane cedex, France
[4] Laboratoire des Sciences du Climat et de l'Environnement (LSCE/IPSL), UMR 8212 (CEA-CNRS-UVSQ), Université Paris-Saclay, 91191 Gif-sur-Yvette Cedex, France.
* corresponding author
**Aumaître, Georges; Keddadouche, Karim.

Abstract

The ^{10}Be, ^{137}Cs and $^{210}Pb_{xs}$ radionuclide fallout has been used for the last several decades to quantify various soil and geomorphological processes and their rates, on different time scales. However, a basic assumption of the studies relying on these radionuclides is that they have a strong affinity for soil particles and that their mobility in soil solution and losses through leaching can be neglected. Another area of the scientific literature deals with the radionuclide mobility in soils as solute. In that context, the objective of this work is to determine the pedological conditions under which this hypothesis of poor solute mobility of radionuclides is valid. To this end, meteoric ^{10}Be, ^{137}Cs and $^{210}Pb_{xs}$ concentrations were measured in six soil profiles representative of 5 soil types contrasted in terms of physico-chemical properties: an Andosol and a Luvisol under pasture, a Ferralsol and a Leptosol under forest and a Podzol both under forest and cultivation. The main soil properties (soil pH, organic carbon (OC) content, particle size distribution and specific extractions) were measured. The <2 µm fraction of the samples was extracted to measure radionuclide activities and undertake mineralogical analysis. Mass balance calculations were made to estimate the potential isotope losses from the soil profiles.

Results show that meteoric ^{10}Be is significantly leached from soils whose pH_w is lower than 5, regardless of the <2 µm particle proportion and Fe oxides content. Significant ^{137}Cs losses

through leaching can generally be neglected except in sandy soils whose pH_w is lower than 4.5 (Podzol). No significant $^{210}Pb_{xs}$ losses were evidenced. For the three radionuclides considered, the major part of their budget is associated with the <2 µm fraction. However, concerning the Andosol, the proportion of radionuclide budget associated with the <2 µm fraction represents less than 40%. With regards to the forested Podzol, two thirds of the $^{210}Pb_{xs}$ budget is associated with the litter. Well-crystallized Fe oxides, illite and interlayered clay minerals as well as allophane, imogolite and other Al-phases in the Andosol and kaolinite in highly weathered acidic soils (Ferralsol) were found to efficiently retain ^{10}Be. Finally, litter degradation and the content of large particulate organic matter were shown to control $^{210}Pb_{xs}$ concentrations in the studied soils. As expected, our results highlight strong contrasts in the retention of the considered isotopes according to soil physico-chemical properties. Accordingly, their mobility and losses through solute transport should be considered when using them for quantifying solid transport and future mass transport models must be improved, in particular through the addition of a solute transfer term. Otherwise, soil redistribution might be strongly overestimated for Podzols, Ferralsols and most probably other acidic tropical soil types (Nitisols, Acrisols, Plinthisols).

Keywords: radionuclides, cosmogenic nuclides, transfers in soils, bearing phases, tracers, fallout

Corresponding author: Sophie Cornu
sophie.cornu@aix.inra.fr
+33 04 42 97 17 96

1. Introduction

Vertical and lateral transfers of matter are significant processes in soil and land formation (e.g. bioturbation, clay translocation, erosion; Wilkinson et al., 2009). Human activities may strongly impact these processes, in particular by increasing soil erosion to a point where soil sustainability is threatened. To quantify the dynamics of these transfers, meteoric ^{10}Be, ^{137}Cs and excess ^{210}Pb ($^{210}Pb_{xs}$) have been extensively used separately over the last decades, only a few recent studies being based on their combination (e.g. Belmont et al., 2014; Jagercikova et al., 2017; Singleton et al., 2017).

Meteoric ^{10}Be (half-life = 1.39 Ma) is a cosmogenic nuclide created in the upper atmosphere by the interaction of primary and secondary cosmic ray particles with oxygen and nitrogen atoms. It is delivered to the terrestrial surface through wet/dry fallout. $^{210}Pb_{xs}$ (half-life = 22.3 years) is produced in the atmosphere by the decay of ^{222}Rn emitted from the soil where it is produced by the ^{238}U decay chain. $^{210}Pb_{xs}$ then returns to the surface of the Earth through wet/dry fallout. This isotope fraction is therefore referred to as unsupported or excess (xs) ^{210}Pb ($^{210}Pb_{xs}$), in contrast to the supported ^{210}Pb fraction, which is produced in the soil. Finally, the radionuclide ^{137}Cs (half-life = 30.2 years) was released and dispersed in the atmosphere during thermonuclear atmospheric tests that occurred between the 1950s and the 1970s and during nuclear power plant accidents (Chernobyl in 1986 and Fukushima Dai-ichi in 2011).

According to their contrasted half-lives and input histories, meteoric ^{10}Be is used to investigate processes over millennial time scales while $^{210}Pb_{xs}$ is rather used to investigate those taking place at centennial timescales and ^{137}Cs is employed for characterizing the processes that occurred in soils after the 1960's. Combining these three radionuclides therefore opens up the possibility to discriminate the natural vs. the anthropogenic impact on solid matter transfers. However, the use of meteoric ^{10}Be, ^{137}Cs and $^{210}Pb_{xs}$ as tracers of solid matter transfer is based

on the assumption that these radionuclides have a strong affinity for soil particles and that their mobilization in dissolved form and the associated losses can be neglected over the period of interest, i.e. millennial and decadal timescales (He and Walling, 1996; Parsons and Foster, 2011; Willenbring and von Blanckenburg, 2010).

Meteoric ^{10}Be adsorbs quickly to the soil mineral surfaces (Willenbring and von Blanckenburg, 2010) because of its high reactivity at pH > 4.5 (Takahashi et al., 1999). It has been demonstrated that ^{137}Cs efficiently adsorbs on soil solid phases such as micaceous clay minerals (Dalgleish and Foster, 1996; Sawhney, 1970, 1964; Schulz, 1960; Vandebroek et al., 2012) with mean K_d values increasing with clay content (Gil-García et al., 2009). Dalgleish and Foster, (1996) demonstrated experimentally that this adsorption was rapid and not site-limited in micaceous soils, but that 2 % of the initial ^{137}Cs input was lost by drainage water. However, their experimental design, and the simulation of high intensity rainfall maximized the generation of preferential flow and thus ^{137}Cs loss in drainage water. Finally, it has also been demonstrated that $^{210}Pb_{xs}$ is strongly adsorbed on mineral particles with a high K_d coefficient of ~10^5 (Matisoff, 2014). Jagercikova et al. (2017) showed that in Eutric Luvisols characterized by a neutral pH and a low organic carbon (OC) concentration, the leaching of these radionuclides can be neglected, as also demonstrated for ^{10}Be through a modeling approach conducted by Campforts et al. (2016). According to these properties, the redistribution of the considered radionuclides with depth is related to that of soil components through bioturbation and clay translocation (Jagercikova et al., 2017).

However, it also exists in the literature a large piece of evidence for some mobility of these radionuclides in solute transfer (e.g. Monaghan et al., 1983; Pavich et al., 1984). Previous studies showed that ^{10}Be may complex with organic macro-molecules to form organo-metallic chemicals (Takahashi et al., 1999) and can be leached from the soil profile under acidic conditions (Egli et al., 2010; Bacon et al., 2012; Campforts et al., 2016). Furthermore, it has

been suggested that ^{137}Cs presents a low K_d in organic soils (>20 % organic matter content) (Gil-García et al., 2009). Vandebroek et al. (2012) showed that the potential soil retention of ^{137}Cs is correlated with pH, CEC and the percentage of silt. They also showed that Podzols, Andosols and Ferralsols have a low affinity for this element. They assumed that this may be due to the lack of micaceous clay in their mineralogy. Moreover, Parsons and Foster (2011) suggested that ^{137}Cs could not be used as a tracer of erosion. Finally, the International Atomic Agency (1998) reported for $^{210}Pb_{xs}$ K_d values lower than those determined in previous studies. This may be due to differences in the results obtained from in-situ and ex-situ experiments (Matisoff, 2014). Accordingly, it may not be justified to neglect their transfer in dissolved fraction in all soil types when these radionuclides are used as environmental tracers and the question remains whether meteoric ^{10}Be, ^{137}Cs and $^{210}Pb_{xs}$ can be used as tracers of soil processes and erosion under all soil types, including those having physico-chemical properties significantly different from those of Luvisols.

To answer this question, we propose a multi-isotopic approach on contrasted soil types to estimate the retention of ^{10}Be, ^{137}Cs and ^{210}Pb as a function of their properties: soil pH, OC concentration, and nature and content of mineral sorbing phases. We focused on five different soil types with contrasted properties and representative of the current pedogenetic functioning on Earth: an Andosol and a Luvisol under pasture, a Ferralsol and a Leptosol under forest and a Podzol both under forest and cultivation. Their ^{10}Be, ^{137}Cs and $^{210}Pb_{xs}$ mass balances were quantified to identify the potential occurrence of losses from the soil profiles. Furthermore, the retention of the considered radionuclides was studied as a function of the soil pH and of the amount and nature of the soil sorbing phases.

2. Materials and methods

2.1. Selection of the studied soils

Soil profiles from long-term experiment sites (Table 1) were sampled: two adjacent Podzols (one pine forested, the other cropped for 18 years); one Andosol under pasture; one forested Leptosol (oak); and, one forested Ferralsol (tropical rainforest). In addition, a Luvisol under pasture previously studied for the three radionuclides (Jagercikova et al., 2017) whose soil properties have been specified was included (Figure 1, Table 1). Since all the studied soils are located on summit positions with a local slope <2 %, or in a plain regarding the Podzol, soil losses by erosion or soil accumulation can reasonably be neglected. The selected soil types cover nearly 30 % of the total continental land area on Earth (Figure 1) and a large range of soil properties in terms of pH, OM and clay content: from OC and < 2 µm rich, basic soils to OC and < 2 µm poor acidic soils (Figure 2).

The studied soils differ by their parent material, depth and content in coarse elements (gravels, cobbles and boulders). The Podzols developed from typical quaternary sand deposits (15 ka – 45 ka years old, Sitzia et al., 2015), the Luvisols from loess deposits (15 ka – 16 ka, Jagercikova et al., 2017), and the Ferralsol from granite (200 ka – 2 Ma, Brossard & Leprun, pers. comm.). None of the aforementioned soils contained coarse elements. Their depth varied between 150 cm for the Podzols and Luvisol, to more than 250 cm for the Ferralsol. The Andosol developed from an alkaline volcanic rock (doreite). It was 85 cm deep with coarse element contents increasing from 5% to 30% with depth. Its age was estimated at 12 ka – 19 ka using the Stockmann et al. (2014) equation. The Leptosol developed from limestone with soil depth varying from 0 to 50 cm. Its content in coarse elements increased with depth, from 15% to 75 %. Both soil depth variability and coarse element content were estimated on a 17 m long and 2 m large trench. The age of the Leptosol was estimated at 7 ka – 12 ka based on experiments of carbonate dissolution and corresponding rates found in the literature (Egli & Fitze, 2001).

For the forested sites, the litter layers were also considered. The Podzol under forest had an acid and thick humus (>5cm), classified as Mor, while the Leptosol and the Ferralsol had thin humus (<2.5cm), classified as Dysmull and Mesomull respectively (Jabiol et al., 2015).

2.2. Sampling

Sampling was conducted in soil pits with stainless steel tools. The sampling was continuous down to the C or R horizon with sampling increments varying between 2 cm and 10 cm with depth. Samples were then oven-dried at 40°C and sieved to 2 mm. Both <2 mm (bulk sample) and >2 mm (coarse elements) fractions were weighed. The proportion of cobbles and boulders and the depth at which the parent rock appears was estimated in the pits. The litter was also sampled under forest.

Soil bulk density was determined for each horizon: by gamma-ray attenuation (NFX31-507:1993) or the excavation-water method for the surface horizons, and by the cylinder method for the deeper layers (ISO-11272:1998; Table S1). For the Leptosol that had a large proportion of coarse elements, bulk density of the < 2mm fractions was estimated by Alexander's (1980) pedotransfer function based on the organic carbon concentration of the bulk soil samples.

2.3 Physico-chemical characterization

Samples were analyzed for their particle-size distribution (Robinson's pipette after water sieving; NF X 31-107), OC concentration (dry combustion; NF ISO 10694), soil water pH (with 1:5 solid:liquid volumetric ratio, NF X 31-107), and total Fe (Fe_t, ICP-OES measurement after HF dissolution, NF X 31-147 method). Fe extracted by the dithionite-citrate-bicarbonate reagent (Fe_d) and oxalate-oxalic acid reagent (Fe_o) was also analyzed. These reagents extract the total Fe oxides and poorly crystalline Fe oxides, respectively. For the Andosol, Si and Al were also analyzed in these extracts (Si_d, Al_d, Si_o, Al_o) in order to quantify the imogolite and allophane content. For the Podzol and the Andosol, Fe, Al and Si were extracted by Na-

pyrophosphate (Fe_p, Al_p, and Si_p), presumed to extract Fe, Al and Si associated with OC. All the analyses were performed at the Soil Analysis Laboratory of INRA (Arras, France). All results are reported in Table S2.

The < 2 µm fraction was collected in water suspension according to the Stokes law, after dispersion in MilliQ® water, at soil pH, without organic matter or cement destructions in order not to release the adsorbed radioelements into the solution (see Jagercikova et al., 2014 for more detailed description). Dried soil was equilibrated in 200 to 300 mL of milliQ water and 20 agate balls of 5 mm diameter in a plastic bottle shacked by inversion for 22 hours as suggested by Balesdent et al. (1991). The mass of dried soil was chosen to obtain 5 g of < 2 µm fraction. The < 2 µm fraction was then sampled according to the Stock's law with no addition of chemical agent until more than 80 % of the total fraction was recovered. This separation was not performed for Podzols for technical reasons. The <2 µm fractions were analyzed for mineralogical composition by X-ray diffraction (X'PertPro MDP, Panalytical) on oriented air-dried (AD), ethylene glycol solvation (EG) slides and heating at 490°C. The concentrations of OC, ^{10}Be, ^{137}Cs and $^{210}Pb_{xs}$ were measured in these fractions.

2.4. Meteoric ^{10}Be, ^{137}Cs and $^{210}Pb_{xs}$ analyses

For meteoric ^{10}Be analyses, ~0.250 g of samples were spiked with 300 µL of a 1000 ppm ^{9}Be carrier (Scharlau; $^{10}Be/^{9}Be \sim 10^{-14}$) and fully digested in a mixture of HF-HNO_3-$HClO_4$ acids. Beryllium was subsequently separated from the resulting solution by successive anionic and cationic resin extraction (DOWEX 1X8, then 50WX8) and precipitation in a basic medium ($Be(OH)_2$). The final precipitate was dried and heated at 800 °C to obtain BeO. Measurements of the $^{10}Be/^{9}Be$ ratios were performed at the French AMS facility ASTER (CEREGE, Aix-en-Provence) operating at 5 MV. ^{10}Be concentrations were calculated from the measured spiked $^{10}Be/^{9}Be$ ratios normalized to the STD-11 standard ($^{10}Be/^{9}Be = (1.191 \pm 0.013) \times 10^{-11}$; Braucher

et al., 2015). Uncertainties in the measured $^{10}Be/^{9}Be$ ratios and in the calculated ^{10}Be concentrations result from counting statistics and instrumental error propagation (Arnold et al., 2010) according to the standard propagation of uncertainties equation. Chemistry blank ratios ranging between 9.36 and 10.00×10^{-15} are at least 1,000 times lower than the sample ratios.

For ^{137}Cs and $^{210}Pb_{xs}$, soil samples were packed into 60-mL pre-tared polyethylene containers and sealed airtight to contain ^{222}Rn and allow in-growth of its decay products. Concentrations in ^{137}Cs (661.6 keV) and ^{210}Pb (46.5 keV) were determined by gamma spectrometry using the very low-background HPGe detectors available at the *Laboratoire des Sciences du Climat et de l'Environnement* (LSCE, Gif sur Yvette, France). $^{210}Pb_{xs}$ was calculated by subtracting the supported concentration (determined using two ^{226}Ra daughters, ^{214}Pb (average count number at 295.2 and 351.9 keV) and ^{214}Bi (609.3 keV) from the total ^{210}Pb concentration (Evrard et al., 2010). The counting time of soil samples varied between 8×10^{4} and 3×10^{5} s. All measured counts were corrected for background levels measured at least every 2 months as well as for detector and geometry efficiency. The radionuclide concentrations (in Bq kg^{-1}) were systematically decay-corrected to a common date, i.e. 15th January 2016. Counting efficiency and quality assurance were conducted using internal and certified IAEA standards (IAEA-444, -135, -375, RGU-1, RGTh-1) prepared in the same containers as the samples. Concentrations of meteoric ^{10}Be, ^{137}Cs and $^{210}Pb_{xs}$ were measured in both the litter and organo-mineral horizons of the soils as well as in the <2 µm fraction.

2.5. Mass balance calculations

2.5.1. Radionuclide inventories

The inventory over the entire soil profile *N* for *n* horizons (in atoms cm^{-2} for meteoric ^{10}Be and in Bq cm^{-2} for ^{137}Cs and $^{210}Pb_{xs}$) was calculated according to equation 1:

$$N = \sum_{i=horizon}^{n} \frac{(100 - \%coarse\ elements_i - \%rock_i)}{100} * \rho_i * \alpha_i * e_i \quad (\mathbf{1})$$

where ρ_i is the soil bulk density (in g cm^{-3}) of the horizon *i,* α_i is the isotope concentration (in atoms g^{-1} for meteoric ^{10}Be and in Bq g^{-1} for ^{137}Cs and ^{210}Pb$_{xs}$) of the horizon *i*, *%coarse elements*$_i$ is the coarse element content of the horizon *i* and *%rock*$_i$ is the proportion of the horizon *i* occupied by rock, in the case of the Leptosol. For the latter, in order to take into account the lateral variability of the depth and coarse element content, calculations were performed at the scale of the trench. Finally, e_i is the horizon thickness (in cm). The total inventories include the litter. As ^{10}Be concentrations were not determined for all the horizons (Table S3), missing concentrations were estimated by linear interpolation for mass balance calculation.

Part of the ^{10}Be concentrations measured in soils may have been produced directly within the mineral lattices (*in situ*-production) and/or, for soils developed from sedimentary materials, may be inherited from pre-deposit exposure to cosmic rays. This contribution must be removed from the total inventory before comparison with the meteoric ^{10}Be input to the soil. The ^{10}Be concentrations produced within quartz grains are generally orders of magnitude lower than the meteoric ^{10}Be concentrations adsorbed on the sediment particles. This is however not the case when ^{10}Be *in situ*-production occurs within calcite (37.9±6.0 atoms g^{-1} yr^{-1}; Braucher et al. (2005)). Thus, *in situ*-produced ^{10}Be concentration was estimated only for the Leptosol. Following Jagercikova et al. (2015), inherited ^{10}Be concentration was estimated as the ^{10}Be concentration measured in the non-pedogenised parent material (C-horizon) for the Podzol .

Finally, assuming no leaching and taking into account the radioactive decay, the calculated inventories were converted into annual input rates for meteoric ^{10}Be and ^{210}Pb$_{xs}$. The accumulation duration of meteoric ^{10}Be was considered as the soil age. For ^{210}Pb$_{xs}$, an

accumulation duration of 150 years was considered (for longer accumulation durations, the annual decay and inputs compensate each other).

2.5.2. Radionuclide input estimation

Radionuclide inputs to the soils were estimated based on literature data. The annual meteoric ^{10}Be inputs were estimated through the equation proposed by Graly et al. (2011), based on latitude and annual rainfall. This equation provides an annual meteoric ^{10}Be input with an associated uncertainty of 20 %. The annual $^{210}Pb_{xs}$ input was estimated based on a linear regression established between the annual precipitation and the annual $^{210}Pb_{xs}$ deposition measurements compiled from Baskaran (2011) and Du et al. (2015). Caesium-137 inputs are based on the values reported by Cambray et al. (1989), UNSCEAR (1982) and Aoyama et al. (2006) for the fallout resulting from nuclear tests. Those related to the Chernobyl accident were estimated from the equation proposed by Roussel-Debel et al. (2007). Inputs associated with the Fukushima Dai-ichi accident in 2011 were shown to be negligible at the sampled sites (≤ 2 Bq m^{-2} ; Evrard et al., 2012).

2.6. Uncertainties propagation

Cumulative uncertainties (reported as $\pm 1\sigma$) are calculated according to the standard error propagation method using the quadratic sum of the relative errors. The uncertainties on inventories include those on individual nuclide measurements, soil bulk densities and coarse element proportions. These two sources of uncertainties (sampling and measurements) represent 22 to 47 % of the total inventories calculated for all the soil types except for the Luvisols that exhibit lower uncertainties for ^{137}Cs and meteoric ^{10}Be, although much larger uncertainties for $^{210}Pb_{(xs)}$. These uncertainties are comparable to the estimation of spatial variability obtained in other studies when quantifying ^{137}Cs inventories at local scales (Lettner et al., 1999; Owens and Walling, 1996; Sutherland et al., 1991; Zhang et al., 2019). We thus

consider that, despite estimations of the radionuclide inventories were performed on a single sampling position for logistical and feasibility reasons, the uncertainty ranges remained reasonable and that they allow concluding on the potential occurrence of radionuclide losses compared to theoretical inputs.

The uncertainties on annual fallout inputs include the uncertainties on inventories and soil ages. For the Ferralsol, since the parent material was not reached during sampling, we added an uncertainty on soil depth. We thus considered a range of soil depth from 2.5 (sampling depth) to 10 m (maximal depth to the fresh rock) to ensure that the inventory - and therefore the theoretical annual input rates without losses - is not minimized. The deepest meteoric ^{10}Be concentration measured (230 - 250 cm) was used for the inventory estimation below 2.5 m.

3. Results

In the following sections, we first describe the soil characteristics and the distribution of meteoric ^{10}Be, ^{137}Cs and $^{210}Pb_{xs}$ concentrations with depth along the profiles. Then, mass balance calculations are presented: (1) to establish the ^{10}Be, ^{137}Cs and $^{210}Pb_{xs}$ inventory proportion contained in the litter and in the < 2 µm fraction; and, (2) to compare the soil inventories to the fallout input estimated from the literature.

3.1. Soil characteristics

The soil pH measured in water (called pH_w hereafter) of the selected soils ranges from basic values in the Leptosol and at the base of the Luvisol (> 7), to slightly acidic values in the Andosol, the cultivated Podzol and the upper horizons of the Luvisol (between 5 and 7), and to acidic values in the forested Podzol and the Ferralsol (< 5, Figure 3A). Higher soil pH_w values in the cultivated Podzol than in the forested Podzol have been induced by farming practices (liming) over the past 18 years (Figure 3A).

While the Podzols, the Luvisol and the Ferralsol are poor in OC (< 40 g kg^{-1} in the topsoil), the Leptosol and the Andosol exhibit high OC concentrations (> 100 g kg^{-1} in the topsoil; Figure 3B). The Podzols OC concentrations decrease in the first 40 cm before increasing in the Bh/Bs horizons at roughly 50-60 cm depth (Figure 3B).

Both Podzols contain less than 30 g kg^{-1} of <2 µm fraction while the Leptosol and the Ferralsol present the highest proportions of this fraction (>300 g kg^{-1}, Figure 3C). The Andosol and the Luvisol have intermediate <2 µm concentrations (100-300 g kg^{-1}). As for OC, the Podzols <2 µm concentrations increase at roughly 50-60 cm depth, in the Bh/Bs horizons (Figure 3C).

The nature of the <2 µm fractions strongly differs among the different soils as shown by the XRD patterns (Figure 4). The Ferralsol's <2 µm fraction is mainly composed of kaolinite (peak at 7.15 Å in AD and EG treatments that disappears at heating) and goethite (peak at 4.85 Å in AD and EG treatments). The occurrence of goethite observed only in this soil (Figure 4) is in agreement with the high Fe_d content extracted from the Ferralsol compared to that found in the other soils (Figure 3D). The Leptosol's <2 µm fraction is composed of both vermiculite and chlorite (peak at 14.32 Å in AD and EG treatments that only partially disappears when heating), illite (peak at 9.99 Å in AD and EG treatment), kaolinite, quartz (peak at 3.34 Å in AD treatment) and interlayered clay minerals (shouldering ranging from 9.99 to 14.32 Å in AD that shifts to values higher than 14.32 Å in EG treatment). It also contains carbonates (< 12 %, Table S2 in supplementary file) and a relatively high concentration in Fe oxides, highlighted by high Fe_d concentrations (Figure 3D). The Luvisol contains smectite (budge centered at 13.21 Å in AD that shifts to 17.45 Å in EG treatment), vermiculite (peak at 14.32 Å in AD and EG treatments that totally disappears at heating), illite, kaolinite and quartz (Figure 4). Its clay assemblage is thus similar to that of the Leptosol with more smectite and illite and less Fe oxides (Figure 3D). The XRD patterns of the Andosol's <2 µm fraction did not evidence the occurrence of any mineral phases (Figure 4). However, the oxalate-oxalic acid reagent extracted

a large content of Fe_o, Si_o and Al_o (Fe_o ranging from 1.2 to 1.7 g $100g^{-1}$; <0.4 g $100g^{-1}$ for the others soils, Table S2 in supplementary file). This is characteristic of poorly ordered minerals, such as allophane and imogolite, that are the main inorganic phases constituting this soil.

The soil types used in our experiments range from acidic soils poor in both < 2 µm fraction and OC to basic soils rich in both < 2 µm fraction and OC. For acidic soils, both < 2 µm poor and rich situations are considered. Soil with slightly acidic to neutral pH are also analyzed with a gradient of < 2 µm and OC concentrations (Figure 2).

3.2. Meteoric ^{10}Be, ^{137}Cs and $^{210}Pb_{xs}$ concentrations

Concentrations of meteoric ^{10}Be vary by an order of magnitude over the studied soils (Figure 5A), with concentrations in the Leptosol and Andosol being the highest and those in the Luvisol, Podzol and Ferralsol the lowest. As for OC and <2 µm particle concentrations, ^{10}Be concentrations decrease in the E horizons of both Podzols, increase in the Bh/Bs before decreasing again in the C horizons. Concentrations in the Ferralsol slightly increase from the surface to 40 cm depth and those in the Luvisol and the Andosol to 70 cm depth. The ^{10}Be concentrations measured in the litter are higher than those found in most of the organo-mineral horizons in the Podzol under forest, while they are significantly lower in the case of Ferralsol and Leptosol.

Concentrations of ^{137}Cs vary by two orders of magnitude over the studied soils (Figure 5B) with concentrations in the Leptosol being the highest and those of the Podzols, Ferralsol and Luvisol the lowest. Podzol litter ^{137}Cs concentrations are significantly higher than those found in the organo-mineral horizons, while they are lower in the case of Leptosol and below the detection limits in the Ferralsol (Figure 5B).

Concentrations of $^{210}Pb_{xs}$ also vary by two orders of magnitude over the studied soils (Figure 5C) with concentrations in the Leptosol being the highest and those in the Podzols and Luvisol

the lowest. Concentrations in the Andosol and Ferralsol are intermediate. Litter $^{210}Pb_{xs}$ concentrations are higher than those found in the organo-mineral horizons.

Concentrations measured in the <2 µm fraction of the organo-mineral horizons are generally higher than those measured in the bulk samples of these horizons (Table 2). Enrichment Factors (EF) around 2 are recorded in the Ferralsol for all radionuclides and in the Andosol for meteoric ^{10}Be (Table 2). The EF recorded in the Leptosol for all radionuclides and in the Andosol for ^{137}Cs and $^{210}Pb_{xs}$ are slightly lower (around 1.5 generally). For the Luvisol, the enrichment factors are generally larger than 3 for the three radionuclides (Table 2).

3.3. Inventories of meteoric ^{10}Be, ^{137}Cs and $^{210}Pb_{xs}$

The inventories of meteoric ^{10}Be, ^{137}Cs and $^{210}Pb_{xs}$ were calculated in each soil (Table 3), as well as their distribution among the litter, <2µm and 2-2000 µm fractions of the organo-mineral horizons (Figure 6). The main observations are:

(1) the meteoric ^{10}Be and ^{137}Cs inventories are the lowest in both Podzols and Ferralsol; considering ^{137}Cs, its inventory in the forested Podzol is lower than that in the cultivated profile; considering $^{210}Pb_{xs}$, the inventories are the lowest in the Luvisol and both Podzols and the highest in the Ferralsol.

(2) the <2 µm fraction contributes to more than 90 % of the total meteoric ^{10}Be and ^{137}Cs inventory in the Ferralsol and Leptosol, supplies about 70 % of these inventories in the Luvisol and provides 26-28 % of these inventories in the Andosol (Figure 6A). Considering $^{210}Pb_{xs}$, the <2 µm fraction contributes to more than 80 % of the total inventory in the Luvisol and in the Leptosol, to 74 % of the total inventory in the Ferralsol, and to 41 % in the Andosol.

(3) the litter contribution to the total $^{210}Pb_{xs}$ inventories of the forest soils is two thirds for the Podzol, one fourth for the Leptosol and negligible for the Ferralsol (Figure 6C). Its contribution to the ^{137}Cs inventory is only significant for the Podzol (about 20%; Figure 6B).

3.4. Comparison of the meteoric ^{10}Be, ^{137}Cs and $^{210}Pb_{xs}$ inventories with theoretical deposition

Theoretically, the radionuclide deposits calculated from the measured inventories should be equal to or lower (in the case of losses) than the theoretical local deposits. This is, however, not the case for the three radionuclides considered in the Leptosol in which the measured inventories are higher by a factor of 2 to 3 than the inputs estimated from the literature (Figure 7, Table 3). The thickness of the Leptosol varies spatially from 0 to 50 cm with large outcrop areas. This variation was taken into account in the inventory calculation. However, the radionuclide concentrations used in the calculation were measured from a pit dug at the place where the soil thickness is the greatest. We assumed that the calculated high inventory values result from radionuclide fallout accumulating in the thickest part of the soil. Indeed, rain water cannot infiltrate into rock outcrops and most probably runs off laterally to the most draining part, i.e. the thickest soil area that thus concentrates the radionuclides. To test this hypothesis, we divide the <2 mm soil mass per square centimeter at the sampled 30-35 cm depth soil profile by the <2 mm soil mass per square centimeter resulting from the integration of the depth variability observed along the trench 17m long over a strip 2m wide. The obtained ratio of 2.5 is considered as a proxy for the flux concentration. Since it is equivalent to the factor obtained between the soil inventory and the theoretical radionuclide input, we considered that it validates our hypothesis and that lateral radionuclide transfer by runoff at the metric scale explained the high inventories recorded for this soil compared to the theoretical input estimation. Such a lateral variability of the inventory due to microtopography was already observed for ^{137}Cs by Foster et al. (1994). In addition, Dalgleish and Foster (1996) also recorded an increase in ^{137}Cs exportation in case of compacted soils leading to a reduction of vertical transfers. The rock outcrop representing an extreme case of this process, their findings confirm our interpretation.

Considering ^{10}Be, significant losses by leaching were recorded in both Podzols and Ferralsol (Figure 7A, Table 3). For ^{137}Cs, losses were recorded only in the Podzol developed under forest (Figure 7B, Table 3). Considering $^{210}Pb_{xs}$, the calculated annual inputs are well correlated with

rainfall, which is in agreement with literature (Figure 7C). We thus conclude that no significant $^{210}Pb_{xs}$ loss was recorded in the studied soils.

4. Discussion

In the Ferralsol and the Podzols, significant losses by leaching of meteoric ^{10}Be were recorded. Other studies already recorded significant ^{10}Be losses in comparable soil types (Tsai et al., 2008; Egli et al., 2010). For these soils, estimation of long-term erosion on the basis of meteoric ^{10}Be inventories would result in an overestimation of more than 70%. In contrast, no losses were observed for $^{210}Pb_{xs}$ and for ^{137}Cs with the exception of the forested Podzol for the latter (Figure 7). For Podzols, the use of ^{137}Cs for estimating erosion may result in an overestimation of this process by a factor of two depending on the history of the pH of the soil since the occurrence of the nuclear tests.

This difference of behavior between meteoric ^{10}Be, on the one hand, and ^{137}Cs and $^{210}Pb_{xs}$, on the other hand, was interpreted as resulting from the difference in duration of the processes traced by the different radionuclides. While meteoric ^{10}Be integrates processes that occurred over several millennia, ^{137}Cs and $^{210}Pb_{xs}$ integrate processes that occurred over the last century or the last several decades.

In addition, ^{137}Cs losses were recorded in the forested Podzol although not in the cultivated profile. The changes in the soil characteristics that occurred over the last few decades have likely stopped the ^{137}Cs mobility in the cultivated Podzol.

The results demonstrate that: (1) losses occur in soils that are highly acidic (Ferralsol, forested Podzol); (2) litter retains/recycles a significant proportion of ^{137}Cs and $^{210}Pb_{xs}$ when its degradation is slow; (3) the <2 µm fraction generally dominates the isotope budget, except in the Andosol. These observations highlight the dominant role of soil pH_w, OC and mineral sorbing phases on the element mobility. In the next sections, we thus consider how these soil

characteristics may affect the retention/mobility of the radionuclides. Finally, we discuss the representativeness of the profiles for other soil types.

4.1. Soil pH_w and isotope mobility in soils

For meteoric ^{10}Be, we observed a linear increase of the concentrations with increasing soil pH_w (Figure 8). This is in agreement with previous research that demonstrates the occurrence of a strong link between meteoric ^{10}Be chemical mobility and soil pH_w (Boschi and Willenbring, 2016; Campforts et al., 2016; Takahashi et al., 1999). Takahashi et al. (1999) demonstrated experimentally that all Be adsorbed on kaolinite at pH > 5.5, unless organic matter is present. Furthermore, Vesely et al. (2002) and You et al. (1989) showed that adsorption on minerals strongly decreases for pH values lower than 5. This explains why losses of meteoric ^{10}Be were only observed in the two soil types having a soil pH_w of 5 or lower, i.e. both Podzols and the Ferralsol (Figure 7A, Table 3), regardless of their < 2 µm particles content and Fe oxides concentrations (Figure 3C, 3D). In contrast, both the Andosol and the Leptosol exhibit higher meteoric ^{10}Be concentrations for a given soil pH_w compared to the other soils (Figure 8) although the estimated annual inputs were quite similar (Figure 7A, Table 3). This is interpreted as resulting from differences in the nature of the solid phases fixing meteoric ^{10}Be (see discussion below). For the Andosol, the upper sample has a meteoric ^{10}Be concentration lower than that expected for the considered soil pH_w (Figure 8), as discussed further below.

For ^{137}Cs, no link between the concentrations in the organo-mineral horizons of the soils and their soil pH_w is observed. This is in agreement with the results of Cherif et al. (2017) who demonstrated by modelling the adsorption of Cs on clay minerals that there was no impact of pH for values higher than 4, corresponding to all the soil types considered here with the exception of the Podzol under forest. The forested Podzol, which has a soil pH_w close to 4 in the upper 50 cm, exhibits a ^{137}Cs inventory half that obtained for its cultivated counterpart, which has a soil pH_w close to 6 over the same depth interval.

In the Podzol under forest, the meteoric ^{10}Be and the ^{137}Cs concentrations depth distribution (Figures 5A, 5B) are similar to the OC depth distribution (Figure 3B) with a peak of concentrations at 50-60 cm. The soil pH_w increases above 4.5 at that depth (Figure 3A) inducing an increase in both OC and <2 µm fraction contents (Figures 3B, 3C), as classically occurring during the podzolisation process. These two changes induce an increase in meteoric ^{10}Be and ^{137}Cs retention. Along the cultivated Podzol, the same behavior is observed for meteoric ^{10}Be although not for ^{137}Cs (Figures 5A, 5B). Since this soil has been cultivated and limed since the ^{137}Cs inputs in the mineral soil, ^{137}Cs did not migrate as it did in the Podzol under forest. Meteoric ^{10}Be was brought to the soil during the entire duration of its formation and could thus migrate to the Bh/Bs horizon before the start of agriculture. This demonstrates that chemical mobility of meteoric ^{10}Be and ^{137}Cs must be considered in forested Podzols, and possibly in other soils with a soil pH_w lower than 4.5, when tracing particle transfer with these radionuclides. No similar potential mobility of $^{210}Pb_{xs}$ was evidenced for this soil.

4.2. Identification of the mineral phases responsible for the radionuclide retention

The three radionuclides are mainly concentrated in the <2µm fraction of the Ferralsol, Luvisol and Leptosol (Figure 6). He and Walling (1996), Shen et al. (2004), Singleton et al. (2017) and Wittmann et al. (2012) observed a significant increase of meteoric ^{10}Be, $^{210}Pb_{xs}$ and ^{137}Cs concentrations with decreasing particle size. This could be interpreted as a consequence of the specific surface area increase with decreasing particle size (He and Walling, 1996) and/or as a difference in affinities for the various minerals contained in the different particle-size fractions. For the Andosol, more than half of the ^{137}Cs and meteoric ^{10}Be and $^{210}Pb_{xs}$ inventory is contained in the 2-2000 µm fraction (Figure 6). Therefore, the nature of the mineral phases contained in the different particle-size fractions is of major importance for controlling the element retention. Singleton et al. (2017) reached the same conclusion, emphasizing the role of secondary minerals in ^{137}Cs, meteoric ^{10}Be and $^{210}Pb_{xs}$ retention.

The nature of the clay minerals (1:1 clay minerals in the Ferralsol versus 2:1 clay minerals in the Luvisol and Leptosol), the amount of Fe oxides (a large amount in the Ferralsol and the Leptosol, versus a negligible amount in both Podzols) vary significantly among the considered soils. Similarly, the presence of allophane and imogolite is recorded only in the Andosol.

Positive correlations between meteoric ^{10}Be concentrations and Fe_d-Fe_o (well-crystallized Fe oxides) concentrations are observed (Figure 9A). Studies by Singleton et al. (2017) and Graly et al. (2010) also showed that concentrations in meteoric ^{10}Be are strongly linked to the Fe oxides content. Nevertheless, no correlation between well-crystallized Fe oxides and meteoric ^{10}Be concentrations was observed for the Ferralsol although it contains significant amounts of this mineral. This was interpreted as the result of meteoric ^{10}Be losses in the Ferralsol due to acid soil pH_w, as discussed above. Besides goethite, kaolinite is the only other mineral contained in the < 2µm fraction. This fraction likely contains most of the meteoric ^{10}Be inventory. We conclude that kaolinite is likely an important sorbing phase in the Ferralsol.

In addition, for a given pH value, more meteoric ^{10}Be is adsorbed in the Leptosol than in the Luvisol (Figure 5A). Both soils have a comparable clay mineral composition but the Luvisol contains a higher amount of illite and smectite. Boschi and Willenbring (2016) showed experimentally that the partition coefficient (K_d) on illite is higher than on other clay minerals. This is in agreement with higher EF in the < 2 µm fraction recorded in the Luvisol (Table 2). However, other mineral phases abundant in the Leptosol have a strong affinity for meteoric ^{10}Be, which could therefore explain the high ^{10}Be concentrations in this soil. As an example, You et al. (1989) demonstrated an affinity of Be for carbonate and the affinity for well-crystallized Fe oxides – more abundant in the Leptosol (Figure 3D) – has been previously discussed.

Regarding ^{137}Cs and $^{210}Pb_{xs}$, higher EF are recorded in the Luvisol that contains 2:1 clay minerals compared to the other soils, less rich in these minerals (Table 2). The 2:1 clay minerals

are indeed considered to efficiently adsorb ^{137}Cs (Cherif et al., 2017; Dumat and Staunton, 1999; Saito et al., 2014; Tamura and Jacobs, 1960; Vandebroek et al., 2012).

In the Andosol, the concentrations in ^{137}Cs, meteoric ^{10}Be and $^{210}Pb_{xs}$ in the <2 µm fraction are relatively high (Table 2) despite the absence of clay minerals. This soil is characterized by the presence of imogolite and allophane. Meteoric ^{10}Be concentrations are linearly correlated to the concentrations in Al and Si extracted by the Tamm reagent (Al_o and Si_o) minus those extracted by Na-pyrophosphate (Al_p and Si_p; Figure 9B), suggesting their adsorption on imogolite, allophane phases and Al oxides. You et al. (1989) found that bauxitic soils, containing Al oxides, had the highest affinity for Be. Barg et al. (1997) showed that Al phases retained a large part of the Be stock. These results are in agreement with our observations. Such an adsorption also explains the strong contribution of the 2 – 2000 µm fraction to the Andosol meteoric ^{10}Be stocks – and most likely also for ^{137}Cs and $^{210}Pb_{xs}$ (Figure 6). Indeed, since allophane and imogolite form very stable silt-sized aggregates, only slightly destroyed by the pretreatment for particle-size distribution analysis, these phases are also found in the 2 – 2000 µm fraction.

4.3. To summarize, illite, Fe oxides, poorly crystalline Al phases and allophane likely provide the main sorbents of meteoric ^{10}Be, as well as kaolinite in highly weathered acidic soil (Ferralsol). Regarding ^{137}Cs and $^{210}Pb_{xs}$, the retention is likely higher on 2:1 clay minerals (Luvisol). *OC and isotope retention in soils*

For the Leptosol and the Andosol that have high OC concentration (>130 g kg^{-1} in the topsoil horizon), strong negative relationships were observed between ^{10}Be and OC concentrations for both soils ($r=-0.998$, $p<0.01$, $n=6$ for the Leptosol; $r=-0.936$, $p<0.01$, $n=10$ for the Andosol). The same relationship was observed for OC rich Luvisols, only for the topsoil horizons and thence without considering the Bt horizon that accumulated ^{10}Be over time (Jagercikova et al., 2015). Campforts et al. (2016) showed by modelling that soils characterized by a high affinity for ^{10}Be do not show any decrease in the topsoil horizons, even in the long-term. It is therefore

likely that the affinity of mineral phases for Be is reduced in the presence of organic coating. This conclusion is supported by the literature. Indeed, Takahashi et al. (1999) showed a decrease in the adsorption on kaolinite in the presence of OC. In addition, a similar decrease in the affinity of clay minerals in the presence of OC was observed for Cs by Dumat and Staunton (1999).

Considering $^{210}Pb_{xs}$, the concentrations in the litter are at least 1.5, up to 27, fold higher than that recorded in the organo-mineral horizon. Additionally, the proportion of the total $^{210}Pb_{xs}$ inventory within the litter increases as the litter degradation slows down (Figure 6): the Podzol Mor humus contains two thirds of the total $^{210}Pb_{xs}$ inventory, the Leptosol Dysmull humus one fourth and this proportion is negligible in the Mesomull humus of the Ferralsol. Moreover, the concentration of $^{210}Pb_{xs}$ in the >2 µm fraction is significantly correlated to the OC concentration among all the studied soils (Figure 10). Such a correlation was already observed for Luvisols by Jagercikova et al., (2014). Lead is known to have a strong affinity for OC (Covelo et al., 2007). Dorr and Munnich (1989) suggested that lead redistribution was directly due to the movement of OM in soils and Teramage et al. (2015) recently proposed to use $^{210}Pb_{xs}$ as a tracer for studying soil OC redistribution at different scales. No correlation was observed between the $^{210}Pb_{xs}$ concentrations and the OC concentration in the <2 µm fraction, strengthening the conclusion of the retention of $^{210}Pb_{xs}$ by litter and large POM. Despite previous evidence of $^{210}Pb_{xs}$ mobilization even in organic-rich soils (Kaste et al., 2005), the current results suggest that most of the $^{210}Pb_{xs}$ inventory is governed by the litter degradation and large POM content.

To summarize: (i) litter degradation and POM content are key drivers of the $^{210}Pb_{xs}$ concentrations in the studied soils; (ii) high OC concentration could reduce the affinity of Be for clay minerals ; (iii) no clear effect of OC on ^{137}Cs budgets was observed in the dataset, despite evidence in the literature of the lower fixation of this element on clay minerals in presence of OC (Dumat and Staunton, 1999).

4.4. Extrapolation of the previous findings to other soil types: what is the representativeness of the chosen profiles on a global scale?

The selected soils cover a large range of soil properties (Figure 2) and represent a large number of soil types. The Ferralsol is characterized by acidic soil pH_w, a large amount of Fe oxide and 1:1 clay minerals. Such characteristics are also found in Plinthosols, Acrisols and Nitisols (IUSS, 2014). The Leptosol is characterized by a large proportion of <2 µm particles with a high content in 2:1 clay minerals, a high content in iron oxides and carbonates. These characteristics can be found in Calcaric Cambisols, Calcisols, Chernozems and Kastanozems. The Luvisol is characterized by a medium content in clay, neutral to slightly acidic soil pH_w, low OC, moderate Fe oxide and 2:1 clay minerals, which are characteristic of most Cambisols. To summarize, the results obtained on the considered soils represent around 54% of the total land surface area of the world.

5. Conclusions

The objective of the current research was to determine the retention - and its drivers - of meteoric ^{10}Be, ^{137}Cs and $^{210}Pb_{xs}$ in contrasted soil types, to better constrain their potential use as tracers for particulate transfers in soils. The results obtained on the studied soils, which can be extrapolated to ~54 % of those found around the world, indicate that:

1. Significant chemical leaching of ^{137}Cs and meteoric ^{10}Be cannot be neglected in sandy soils with soil $pH_w < 4.5$ for ^{137}Cs and in soils with soil $pH_w < 5$ for meteoric ^{10}Be, regardless of the < 2 µm and Fe oxides content. Significant losses of $^{210}Pb_{xs}$ by leaching are unlikely. For these soils, soil redistribution might be strongly overestimated if these losses are not considered. As an example, for Podzols and Ferralsols, the estimation of long-term erosion on the basis of meteoric ^{10}Be inventories would result in an overestimation of more than 70%. In addition, for Podzols, the use of ^{137}Cs for the estimation of the erosion may result

in an overestimation of erosion by a factor of two depending on the history of the pH of the soil since the occurrence of the nuclear tests.

2. The three radionuclides are mainly concentrated in the <2 µm fraction with the exception of the Andosol. Regarding meteoric ^{10}Be, well-crystallized Fe oxides, illite and interlayered clay minerals likely act as a sink, as well as allophane, imogolite and other Al-phases in the Andosol. Kaolinite also likely retains ^{10}Be in highly weathered acidic soils. Regarding ^{137}Cs and possibly $^{210}Pb_{xs,}$ they are particularly retained by 2:1 clay minerals, as already observed in the literature.
3. Litter degradation and OC concentrations in the >2 µm fraction are key parameters controlling the $^{210}Pb_{xs}$ concentrations in the uppermost soil horizons.

In addition, radionuclide behavior in basic soils depleted in < 2 µm fractions and either rich or poor in OC, such as Arenosols with a calcareous parent material, should still be addressed, as well as in acidic soils enriched in both < 2 µm and OC, such as Histosols. Besides, the impact of other major pedogenic processes such as reduction and salinization on the radionuclide behavior was not considered in this study. These processes are major soil formation processes in Gleysols, Planosols, Stagnosols, Solonetz and Solonchaks.

Finally, we suggest that the use of the studied radionuclides to trace solid transfers requires the preliminary assessment of the radionuclide redistribution by solute transfer within the considered soil profiles. This is a prerequisite for their use in tracing particle transfers in soil profiles that are generally modelled without considering any solute transfer. Models should thus be improved through the addition of a solute transfer term to the classical particle transfer (e.g. Campforts et al. (2016) for meteoric ^{10}Be). This approach could be combined to the multi-isotopic model developed by Jagercikova et al. (2017).

Acknowledgements

This research was conducted in the framework of the Agriped project (ANR-10-BLANC-605) and the DeDyCas project (ANR 14-CE01-0004) supported by the French National Research Agency (ANR). The authors are grateful to the following research teams for having kindly provided the results of their long-term experiments and the associated data: INRA of Mons-en-Chaussée, INRA-AgroParistech ECOSYS, Arvalis, INRA Unité Experimentale Forêt Pierroton, INRA ISPA (Pierroton forest reserve and fertilization experiment), OSU-Pytheas (O3HP LTER in Saint-Michel l'Observatoire), INRA UREP, SOERE ACBB and LAMA-IMAGO-IRD-Cayenne (French Guyana). The ASTER AMS national facility (CEREGE, Aix-en-Provence), is supported by the INSU/CNRS, the ANR through the "Projets thématiques d'excellence" program for the "Equipements d'excellence" ASTER-CEREGE action (ANR-10-EQPX-24-1) and IRD.

References

Alexander, E.B., 1980. Bulk densities of California soils in relation to other soil properties. Soil Sci. Soc. Am. J. 44, 689–692.

Aoyama, M., Hirose, K., Igarashi, Y., 2006. Re-construction and updating our understanding on the global weapons tests 137Cs fallout. J. Environ. Monit. 8, 431–8. https://doi.org/10.1039/b512601k

Arnold, M., Merchel, S., Bourlès, D.L., Braucher, R., Benedetti, L., Finkel, R.C., Aumaître, G., Gottdang, A., Klein, M., 2010. The French accelerator mass spectrometry facility ASTER: Improved performance and developments. Nucl. Instruments Methods Phys. Res. Sect. B Beam Interact. with Mater. Atoms 268, 1954–1959. https://doi.org/10.1016/j.nimb.2010.02.107

Bacon, A.R., Richter, D. de B., Bierman, P.R., Rood, D.H., 2012. Coupling meteoric 10Be

with pedogenic losses of 9Be to improve soil residence time estimates on an ancient North American interfluve. Geology 40, 847–850. https://doi.org/10.1130/G33449.1

Balesdent, J., Pétraud, J.P., Feller, C., 1991. Effet des ultrasons sur la distribution granulométrique des matières organiques des sols. Sci. du sol 29, 95–106.

Barg, E., Lal, D., Pavich, M.J., Caffee, M.W., Southon, J.R., 1997. Beryllium geochemistry in soils: Evaluation of 10Be/9Be ratios in authigenic minerals as a basis for age models. Chem. Geol. 140, 237–258. https://doi.org/10.1016/S0009-2541(97)00051-X

Baskaran, M., 2011. Po-210 and Pb-210 as atmospheric tracers and global atmospheric Pb-210 fallout: A Review. J. Environ. Radioact. 102, 500–513. https://doi.org/10.1016/j.jenvrad.2010.10.007

Belmont, P., Willenbring, J.K., Schottler, S.P., Marquard, J., Kumarasamy, K., Hemmis, J.M., 2014. Toward generalizable sediment fingerprinting with tracers that are conservative and nonconservative over sediment routing timescales 1479–1492. https://doi.org/10.1007/s11368-014-0913-5

Boschi, V., Willenbring, J., 2016. The effect of pH, organic ligand chemistry and mineralogy on the sorption of beryllium over time. Environ. Chem. 13, 711–722.

Braucher, R., Benedetti, L., Bourlès, D.L., Brown, E.T., Chardon, D., 2005. Use of in situ-produced 10Be in carbonate-rich environments: A first attempt. Geochim. Cosmochim. Acta 69, 1473–1478. https://doi.org/10.1016/j.gca.2004.09.010

Braucher, R., Guillou, V., Bourlès, D.L., Arnold, M., Aumaître, G., Keddadouche, K., Nottoli, E., 2015. Preparation of ASTER in-house $^{10}Be/^{9}Be$ standard solutions. Nucl. Instruments Methods Phys. Res. Sect. B Beam Interact. with Mater. Atoms 361, 335–340. https://doi.org/10.1016/j.nimb.2015.06.012

Cambray, R.S., Playford, K., Carpenter, R.C., 1989. Radioactive fallout in air and rain: results to the end of 1988. UK At. Energy Auth. Rep. AERE-R 10155, HMSO.

Campforts, B., Vanacker, V., Vanderborght, J., Baken, S., Smolders, E., Govers, G., 2016. Simulating the mobility of meteoric 10Be in the landscape through a coupled soil-hillslope model (Be2D). Earth Planet. Sci. Lett. 439, 143–157. https://doi.org/10.1016/j.epsl.2016.01.017

Cherif, M.A., Martin-garin, A., Gérard, F., Bildstein, O., 2017. A robust and parsimonious model for caesium sorption on clay minerals and natural clay materials. Appl. Geochemistry 87, 22–37. https://doi.org/10.1016/j.apgeochem.2017.10.017

Covelo, E.F., Vega, F.A., Andrade, M.L., 2007. Competitive sorption and desorption of heavy metals by individual soil components 140, 308–315. https://doi.org/10.1016/j.jhazmat.2006.09.018

Dalgleish, H.Y., Foster, I.D.L., 1996. Cs-137 losses from a loamy surface water gleyed soil (Inceptisol): a laboratory simulation experiment. Catena 26, 227–245.

Dorr, H., Munnich, K., 1989. Downward movement of soil organic matter and its influence on trace element transport (210Pb, 137Cs) in the soil. Radiocarbon 31, 655–663.

Du, Juan, Du, Jinzhou, Baskaran, M., Bi, Q., Huang, D., Jiang, Y., 2015. Temporal variations of atmospheric depositional fluxes of 7Be and 210Pb over 8 years (2006-2013) at Shangai, China, and synthesis of global fallout data. J. Geophys. Res. Atmos. 4323–4339. https://doi.org/10.1002/2014JD022807

Dumat, C., Staunton, S., 1999. Reduced adsorption of caesium on clay minerals caused by various humic substances. J. Environ. Monit. 46, 187–200.

Egli, M., Brandová, D., Böhlert, R., Favilli, F., Kubik, P.W., 2010. 10Be inventories in Alpine soils and their potential for dating land surfaces. Geomorphology 119, 62–73. https://doi.org/10.1016/j.geomorph.2010.02.019

Egli, M., Fitze, P., 2001. Quantitative aspects of carbonate leaching of soils with differing ages and climates. Catena 46, 35–62. https://doi.org/10.1016/S0341-8162(01)00154-0

Evrard, O., Némery, J., Gratiot, N., Duvert, C., Ayrault, S., Lefèvre, I., Poulenard, J., Prat, C., Bonté, P., Esteves, M., 2010. Sediment dynamics during the rainy season in tropical highland catchments of central Mexico using fallout radionuclides. Geomorphology 124, 42–54. https://doi.org/10.1016/j.geomorph.2010.08.007

Evrard, O., Van Beek, P., Gateuille, D., Pont, V., Lefèvre, I., Lansard, B., Bonté, P., 2012. Evidence of the radioactive fallout in France due to the Fukushima nuclear accident. J. Environ. Radioact. 114, 54–60. https://doi.org/10.1016/j.jenvrad.2012.01.024

Foster, I.D.L., Dalgleish, H., Dearing, J.A., Jones, E.D., 1994. Quantifying soil erosion and sediment transport in drainage basins; some observations on the use of 137Cs., in: Olive, L.J., Loughran, R.J., Kesby, J.A. (Eds.), Variability in Stream Erosion and Sediment Transport. Wailingford, U.K., pp. 55–64.

Gil-García, C., Rigol, A., Vidal, M., 2009. New best estimates for radionuclide solid-liquid distribution coefficients in soils, Part 1: Radiostrontium and radiocaesium. J. Environ. Radioact. 100, 690–696. https://doi.org/10.1016/j.jenvrad.2008.10.003

Graly, J.A., Bierman, P.R., Reusser, L.J., Pavich, M.J., 2010. Meteoric 10Be in soil profiles - A global meta-analysis. Geochim. Cosmochim. Acta 74, 6814–6829. https://doi.org/10.1016/j.gca.2010.08.036

Graly, J.A., Reusser, L.J., Bierman, P.R., 2011a. Short and long-term delivery rates of meteoric 10Be to terrestrial soils. Earth Planet. Sci. Lett. 302, 329–336. https://doi.org/10.1016/j.epsl.2010.12.020

Graly, J.A., Reusser, L.J., Bierman, P.R., 2011b. Short and long-term delivery rates of meteoric 10Be to terrestrial soils. Earth Planet. Sci. Lett. 302, 329–336. https://doi.org/10.1016/j.epsl.2010.12.020

He, Q., Walling, D.E., 1996. Interpreting particle size effects in the adsorption of 137Cs and unsupported 210Pb by mineral soils and sediments. J. Environ. Radioact. 30, 117–137.

https://doi.org/10.1016/0265-931X(96)89275-7

International Atomic Agency, 1998. Use of 137 Cs in the study of soil erosion and sedimentation 13–16.

IUSS, 2014. World reference base for soil classification 2014. Food Agric. Organ. United Nations, Rome.

Jabiol, B., Brêthes, A., Brun, J.J., Jean-françois, P., Toutain, F., Zanella, A., Aubert, M., Bureau, F., Jabiol, B., Brêthes, A., Brun, J.J., Jean-françois, P., Toutain, F., 2015. Typologie des formes d ' humus forestières (sous climats tempérés) To cite this version : HAL Id : hal-01184636 Typologie des formes d ' humus forestières.

Jagercikova, M., Cornu, S., Bourlès, D., Antoine, P., Mayor, M., Guillou, V., 2015. Understanding long-term soil processes using meteoric 10Be: A first attempt on loessic deposits. Quat. Geochronol. 27, 11–21. https://doi.org/10.1016/j.quageo.2014.12.003

Jagercikova, M., Cornu, S., Bourlès, D., Evrard, O., Hatté, C., Balesdent, J., 2017. Quantification of vertical solid matter transfers in soils during pedogenesis by a multi-tracer approach. J. Soils Sediments 17, 408–422. https://doi.org/10.1007/s11368-016-1560-9

Jagercikova, M., Evrard, O., Balesdent, J., Lefèvre, I., Cornu, S., 2014. Modeling the migration of fallout radionuclides to quantify the contemporary transfer of fine particles in Luvisol profiles under different land uses and farming practices. Soil Tillage Res. 140, 82–97. https://doi.org/10.1016/j.still.2014.02.013

Kaste, J.M., Friedland, A.J., Miller, E.K., 2005. Potentially mobile leaf fractions in montane organic-rich horizons. Environ. Stud. 139–154.

Lettner, H., Bossew, P., Hubmer, A.K., 1999. Spatial variability of fallout Caesium-137 in Austrian alpine regions. J. Environ. Radioact. 47, 71–82. https://doi.org/10.1016/S0265-931X(99)00023-5

Matisoff, G., 2014. 210Pb as a tracer of soil erosion, sediment source area identification and particle transport in the terrestrial environment. J. Environ. Radioact. 138, 343–354. https://doi.org/10.1016/j.jenvrad.2014.03.008

Monaghan, M.C., Krishnaswami, S., Thomas, J.H., 1983. 10Be concentrations and the long-term fate of particle-reactive nuclides in five soil profiles from California. Earth Planet. Sci. Lett. 65, 51–60. https://doi.org/10.1016/0012-821X(83)90189-9

Owens, P.N., Walling, D.E., 1996. Spatial variability of caesium-137 inventories at reference sites: An example from two contrasting sites in England and Zimbabwe. Appl. Radiat. Isot. 47, 699–707. https://doi.org/10.1016/0969-8043(96)00015-2

Parsons, A.J., Foster, I.D.L., 2011. Earth-Science Reviews What can we learn about soil erosion from the use of Cs ? Earth Sci. Rev. 108, 101–113. https://doi.org/10.1016/j.earscirev.2011.06.004

Pavich, M.J., Brown, L., Klein, J., Middleton, R., 1984. 10Be accumulation in a soil chronosequence. Earth Planet. Sci. Lett. 68, 198–204. https://doi.org/10.1016/0012-821X(84)90151-1

Roussel-Debel, S., Renaud, P., Métivier, J.M., 2007. 137Cs in French soils: Deposition patterns and 15-year evolution. Sci. Total Environ. 374, 388–398. https://doi.org/10.1016/j.scitotenv.2006.12.037

Saito, T., Makino, H., Tanaka, S., 2014. Geochemical and grain-size distribution of radioactive and stable cesium in Fukushima soils : implications for their long-term behavior. J. Environ. Radioact. 138, 11–18. https://doi.org/10.1016/j.jenvrad.2014.07.025

Sawhney, B., 1970. Potassium and cesium ion selectivity in relation to clay mineral structure. Clays Clay Miner. 18, 47–52.

Sawhney, B., 1964. Sorption and Fixation of Microquantities of Cesium by Clay Minerals:

Effect of Saturating Cations. Soil Sci. Soc. Am. J. 28, 183–186.

Schulz, R., 1960. On the soil chemistry of cesium 137. Soil Sci. 89, 16–27.

Shen, C., Beer, J., Kubik, P.W., Suter, M., Borkovec, M., Liu, T.S., 2004. Grain size distribution,10Be content and magnetic susceptibility of micrometer-nanometer loess materials. Nucl. Instruments Methods Phys. Res. B. 223–224, 613–617. https://doi.org/10.1016/j.nimb.2004.04.113

Singleton, A.A., Schmidt, A.H., Bierman, P.R., Rood, D.H., Neilson, T.B., Greene, E.S., Bower, J.A., Perdrial, N., 2017. Effects of grain size, mineralogy, and acid-extractable grain coatings on the distribution of the fallout radionuclides 7Be, 10Be, 137Cs, and 210Pb in river sediment. Geochim. Cosmochim. Acta 197, 71–86. https://doi.org/10.1016/j.gca.2016.10.007

Sitzia, L., Bertran, P., Bahain, J.J., Bateman, M.D., Hernandez, M., Garon, H., de Lafontaine, G., Mercier, N., Leroyer, C., Queffelec, A., Voinchet, P., 2015. The quaternary coversands of southwest France. Quat. Sci. Rev. 124, 84–105. https://doi.org/10.1016/j.quascirev.2015.06.019

Stockmann, U., Minasny, B., McBratney, A.B., 2014. How fast does soil grow? Geoderma 216, 48–61. https://doi.org/10.1016/j.geoderma.2013.10.007

Sutherland, R.A., Kowalchuk, T.A., de Jong, E., 1991. Cesium-137 estimates of sediment redistribution wind. Soil Sci. 151, 387–396.

Takahashi, Y., Minai, Y., Ambe, S., Makide, Y., Ambe, F., 1999. Comparison of adsorption behavior of multiple inorganic ions on kaolinite and silica in the presence of humic acid using the multitracer technique. Geochim. Cosmochim. Acta 63, 815–836. https://doi.org/10.1016/S0016-7037(99)00065-4

Tamura, T., Jacobs, D.G., 1960. Structural implications in cesium sorption. Health Phys. 2, 391–398.

Teramage, M.T., Onda, Y., Wakiyama, Y., Kato, H., Kanda, T., Tamura, K., 2015. Atmospheric (210)Pb as a tracer for soil organic carbon transport in a coniferous forest. Environ. Sci. Process. Impacts 17, 110–9. https://doi.org/10.1039/c4em00402g

Tsai, H., Maejima, Y., Hseu, Z.Y., 2008. Meteoric 10Be dating of highly weathered soils from fluvial terraces in Taiwan. Quat. Int. 188, 185–196. https://doi.org/10.1016/j.quaint.2007.06.007

UNSCEAR, 1982. Ionizing radiation: Sources and biological effects. https://doi.org/10.1080/09553008314550691

Vandebroek, L., Van Hees, M., Delvaux, B., Spaargaren, O., Thiry, Y., 2012. Relevance of Radiocaesium Interception Potential (RIP) on a worldwide scale to assess soil vulnerability to 137Cs contamination. J. Environ. Radioact. 104, 87–93. https://doi.org/10.1016/j.jenvrad.2011.09.002

Vesely, J., Norton, S.A., Skrivan, P., Majer, V., Kram, P., Navratil, T., Kaste, J.M., 2002. Environmental chemistry of beryllium. Rivers Mineral. Geochemistry Rev. Miner. Geochem. 50, 291–3187. https://doi.org/10.2138/rmg.2002.50.7

Wilkinson, M.T., Richards, P.J., Humphreys, G.S., 2009. Breaking ground: Pedological, geological, and ecological implications of soil bioturbation. Earth-Science Rev. 97, 257–272. https://doi.org/10.1016/j.earscirev.2009.09.005

Willenbring, J.K., von Blanckenburg, F., 2010. Meteoric cosmogenic Beryllium-10 adsorbed to river sediment and soil: Applications for Earth-surface dynamics. Earth-Science Rev. 98, 105–122. https://doi.org/10.1016/j.earscirev.2009.10.008

Wittmann, H., Von Blanckenburg, F., Bouchez, J., Dannhaus, N., Naumann, R., Christl, M., Gaillardet, J., 2012. The dependence of meteoric10Be concentrations on particle size in Amazon River bed sediment and the extraction of reactive10Be/9Be ratios. Chem. Geol. 318–319, 126–138. https://doi.org/10.1016/j.chemgeo.2012.04.031

You, C.F., Lee, T., Li, Y.H., 1989. The partition of Be between soil and water. Chem. Geol. 77, 105–118. https://doi.org/10.1016/0009-2541(89)90136-8

Zhang, X.C., Polyakov, V.O., Liu, B.Y., Nearing, M.A., 2019. Quantifying geostatistical properties of 137Cs and 210Pbex at small scales for improving sampling design and soil erosion estimation. Geoderma 334, 155–164. https://doi.org/10.1016/j.geoderma.2018.08.002

Table and figure captions

Table 1 – Characteristics of the studied sites

Table 2 – Radionuclides and OC concentrations in the < 2 µm fraction of the studied soils and enrichment factors (EF) in this fraction compared to the concentration in the bulk soil.

Table 3 – Calculated ^{137}Cs, $^{210}Pb_{xs}$ and ^{10}Be stocks in the studied soils and estimated input from the literature

Figure 1 – Location of the study sites (red dots) and surface occupied by the considered soil types worldwide. AN stands for Andosol, FR for Ferralsol, LP for Leptosol, LV for Luvisol and PZ for Podzols.

Figure 2 – 3D representation of soil pH_w, OC and <2 µm concentrations in the considered soils.

Figure 3 – Depth distribution of (A) the soil pH_w, (B) the organic carbon (OC), (C) < 2 µm fraction and (D) Fe_d concentrations. Note the difference in scale according to the soil considered for OC, < 2 µm fraction and Fe_d.

Figure 4 – XRD patterns of the < 2 µm fraction on (A) oriented air-dried (AD) slide and (B) ethylene glycol solvation (EG) slide. The depth of the analyzed samples ranges from 30 to 50 cm. V is for vermiculite, I for illite, K for kaolinite, G for goethite and Q for quartz.

Figure 5 – Depth distribution of meteoric ^{10}Be (A), ^{137}Cs (B) and $^{210}Pb_{xs}$ (C) concentrations. Dotted red lines indicate the limits between the litter and the organo-mineral horizons. Note the difference in scale according to the soil considered. For Podzols in (B) and (C), the top scale of for the soil horizons and the bottom scale is for the litter horizons.

Figure 6 – Depth distribution of meteoric ^{10}Be (A), ^{137}Cs (B) and $^{210}Pb_{xs}$ (C) stocks and their distribution among litter, < 2µm and 2-2000 µm fractions. Data for Luvisol are derived from Jagercikova et al. (2015, 2014b).

Figure 7 - (A) Annual ^{10}Be inputs calculated from the measured stocks as a function of those estimated from Graly et al. (2011); (B) Measured ^{137}Cs stocks as a function of the ^{137}Cs inputs estimated from the literature (Aoyama et al., 2006; Cambray et al., 1989; Roussel-Debel et al., 2007; UNSCEAR, 1982). (C) Linear regression between measured $^{210}Pb_{xs}$ annual deposits from the literature (Baskaran, 2011; Du et al., 2015) and the annual amount of rainfall. Annual deposits estimated from the soil stocks for the different sites are also reported considering the rainfall of the site. Data for Luvisol derived from Jagercikova et al. (2014b, 2015). The shaded area represents 95% confidence interval.

Figure 8 – Meteoric ^{10}Be concentrations as a function of the soil pH_w. "Andosol surface" is not included in the Andosol relationship. "Other soils" include both Podzols, the Luvisol and the Ferralsol. Shaded areas represent 95% confidence interval.

Figure 9 – (A) Meteoric ^{10}Be concentrations as a function of well-crystallized Fe oxides (Fe_d-Fe_o). "Other soils" include both Podzols and the Luvisol. (B) Meteoric ^{10}Be concentrations as a function of Al and Si extracted by Tamm (Al_o, Si_o) minus those extracted by Na-pyrophosphate (Al_p, Si_p) in the Andosol. Shaded areas represent 95% confidence interval.

Figure 10 – $^{210}Pb_{xs}$ concentrations in the > 2 µm fraction as a function of the OC concentration in the > 2 µm fraction. The shaded area represents 95% confidence interval.

Table S1 – Bulk densities of the sampled soils (2 pages).

Table S2 – Soil physicochemical characteristics (3 pages).

Table S3 – Radionuclide concentrations in the studied bulk soils (2 pages).

Table 1 – Characteristics of the studied sites

WRB soil type	Podzol 1&2	Andosol	Leptosol	Ferralsol	Luvisol*
Site name	Pierroton *INRA*	Laqueuille *INRA*	St Michel l'Observatoire *O3HP*	Rocoucoua	Mons *ORE ACBB*
Geographic coordinates	44°44'33''N 0°47'04''O	45°38'38''N 2°43'59''E	43°56'06''N 5°42'37''E	5°24'39''N 53°18'55''O	49°52'01''N 3°01'53''E
Altitude	59m	1035m	682m	84m	88m
Mean annual rainfall	890mm	1375mm	886mm	2781mm	680mm
Mean annual temperature	12.6°C	7.8°	11.8°C	23.5°	10.4°C
Wind direction	W to WSW NNE à ESE	N and S	N–NW E to S	ENE	ENE–W–SSW
Distance from the coast	38 km	305 km	67 km	14 km	115 km
Parent material	Sand	Doreite	Calcarous rock	Granite	3 lœss deposits
Estimated soil age range	44.8ka–15ka	11.9ka–19.1ka	7.6ka–11.5ka	200 kyr–2 Myr	16ka–15ka
Soil depth	150 cm	85 cm	From 0 to 50 cm	> 250 cm	120 cm
Stoniness	–	5 to 30%	15 to 75 %	–	–
Size of the gravels and stones	–	cm to m	cm to dm	–	–
Slope	< 1°	3°	1.7°	2°	< 1°
Hillslope position	plain	summit	summit	plateau	plateau
Number of sampled profiles	2	1	1	1	1
Land use	Forest (1) and cultivated for the last 22 years (2)	Pasture	Forest	Forest	Pasture for the last 72 years
Litter type	Mor	-	Dysmull	Mesomull	-
Sampling date	May 2014	September 2015	Agust 2015	January 2016	March 2011

*according to Jagercikova et al. (2014b, 2015)

Table 2: Isotopes and OC concentrations in the < 2 µm fraction of the studied soils and enrichment factors (EF) in this fraction compared to the concentration in the bulk soil

Site	Depth in cm	^{137}Cs (Bq kg^{-1})	EF**	$^{210}Pb_{xs}$ (Bq kg^{-1})	EF	meteoric ^{10}Be (10^8 atoms.g^{-1})	EF	OC (g kg^{-1})	EF
Luvisol*	0-2	16.6 ± 0.7	4.4	38.5 ± 4.6	2.7	8.9 ± 0.3	3.7	32.7 ± 1.0	1.0
	2-4	16.4 ± 0.7	4.2	25.7 ± 4.0	3.0	8.9 ± 0.3	3.5	28.0 ± 0.8	1.0
	18-20	16.5 ± 0.5	4.6	24.7 ± 3.0	5.9	9.6 ± 0.3	3.6	16.3 ± 0.5	1.0
	45-50	< 1.3		< 9.1		9.7 ± 0.3	3.1	6.9 ± 0.3	1.3
	60-65	< 0.6		< 4.6		8.4 ± 0.2	2.4	2.5 ± 0.1	0.7
	82-92	< 0.9		< 6.7		8.9 ± 0.2	2.6	1.4 ± 0.1	0.6
	102-112	nd		nd		8.8 ± 0.2	2.7	1.5 ± 0.1	0.8
Leptosol	0-2	438.4 ± 3.1	1.7	499.8 ± 10.2	1.5	34.2 ± 0.6	1.7	118.5 ± 1.5	0.8
	6-8	36.0± 0.9	0.8	< 10.9		51.5 ± 0.9	1.8	27.3 ± 0.4	0.6
	30-35	< 1.3		< 10.8		52.8 ± 1.0	1.7	16.6 ± 0.2	0.8
Andosol	0-2	28.2 ± 0.8	1.6	134.3 ± 5.1	1.6	12.8 ± 0.2	1.9	211.0 ± 2.6	1.5
	6-8	40.0 ± 0.8	1.5	102.7 ± 4.3	1.5	13.4 ± 0.2	1.9	192.9 ± 2.3	1.6
	40-45	< 1.0		18.4 ± 3.6		24.5 ± 0.4	2.0	89.7 ± 1.1	1.8
	80-90	< 1.0		23.7 ± 3.7		19.2 ± 0.4	2.6	65.1 ± 0.8	2.3
Ferralsol	0-2	14.6 ± 0.7	3.1	150.7 ± 6.2	2.0	1.2 ± 0.0	3.1	52.4 ± 0.6	1.2
	16-18	6.4 ± 0.6	2.3	14.4 ± 4.7	1.0	1.2 ± 0.0	2.1	25.2 ± 0.3	1.4
	45-50	< 1.2		< 8.1		1.2 ± 0.0	1.7	13.0 ± 0.1	1.3
	150-170	< 0.8		< 5.9		1.0 ± 0.0	2.0	6.0 ± 0.1	1.3

*According to Jagercikova et al. (2014, 2015)

** Calculated as the activity in the fraction <2 µm / activity in the bulk sample

Table 3 – Calculated and estimated ^{137}Cs, $^{210}Pb_{xs}$ and ^{10}Be stocks in the studied soils.

Soil	^{137}Cs stock (Bq m^{-2})	Estimated ^{137}Cs stock from literature* (Bq m^{-2})	$^{210}Pb_{(xs)}$ stock (Bq m^{-2})	$^{210}Pb_{(xs)}$ input rate† (Bq m^{-2} yr^{-1})	^{10}Be stock (x10^{8} atoms cm^{-2})	Inherited or *in–situ* ^{10}Be stocks (x10^{8} atoms cm^{-2})	^{10}Be input rate‡ (x10^{6} atoms cm^{-2} yr^{-1})	Estimated ^{10}Be input rate from literature§ (x10^{6} atoms cm^{-2} yr^{-1})
Luvisol**	1850 ± 184	2218 ± 373	1325 ± 1377	59 ± 62	505 ± 79	333 ± 52	1.14 ± 0.55	1.39 ± 0.28
Podzol 1	810 ± 309	1846 ± 470	2263 ± 1081	101 ± 48	100 ± 24	80 ± 5	0.14 ± 0.15	1.79 ± 0.36
Podzol 2	1627 ± 386	1846 ± 470	2824 ± 933	127 ± 42	172 ± 38	85 ± 5	0.48 ± 0.36	1.79 ± 0.36
Andosol	3079 ± 969	2178 ± 373	6095 ± 2191	273 ± 98	409 ± 114	Negligible	2.98 ± 1.42	2.78 ± 0.56
Leptosol	5521 ± 1441	2556 ± 540	5048 ± 1435	226 ± 64	294 ± 76	48 ± 20	4.61 ± 2.02	1.76 ± 0.35
Ferralsol	1024 ± 393	509 ± 57	8192 ± 3223	367 ± 145	166 ± 37	Negligible	0.21 ± 0.20	1.76 ± 0.35

* Based on Aoyama et al. (2006), Cambray et al. (1989), Roussel-Debel et al. (2007) and UNSCEAR (1982).
† Calculated with $^{210}Pb_{xs}$ stock and $^{210}Pb_{xs}$ half-life
‡ Calculated with ^{10}Be stock and soil age
§ Based on Graly et al. (2011)
** According to Jagercikova et al. (2014, 2015)

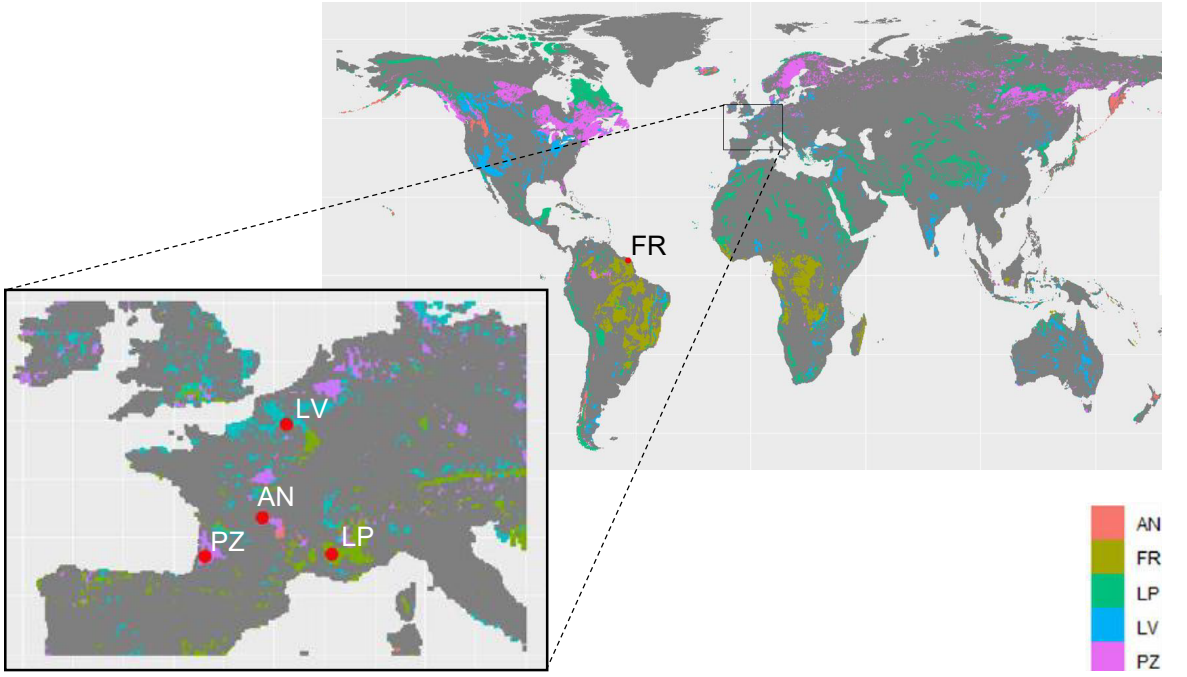
FR
LV
AN
PZ
LP
AN
FR
LP
LV
PZ

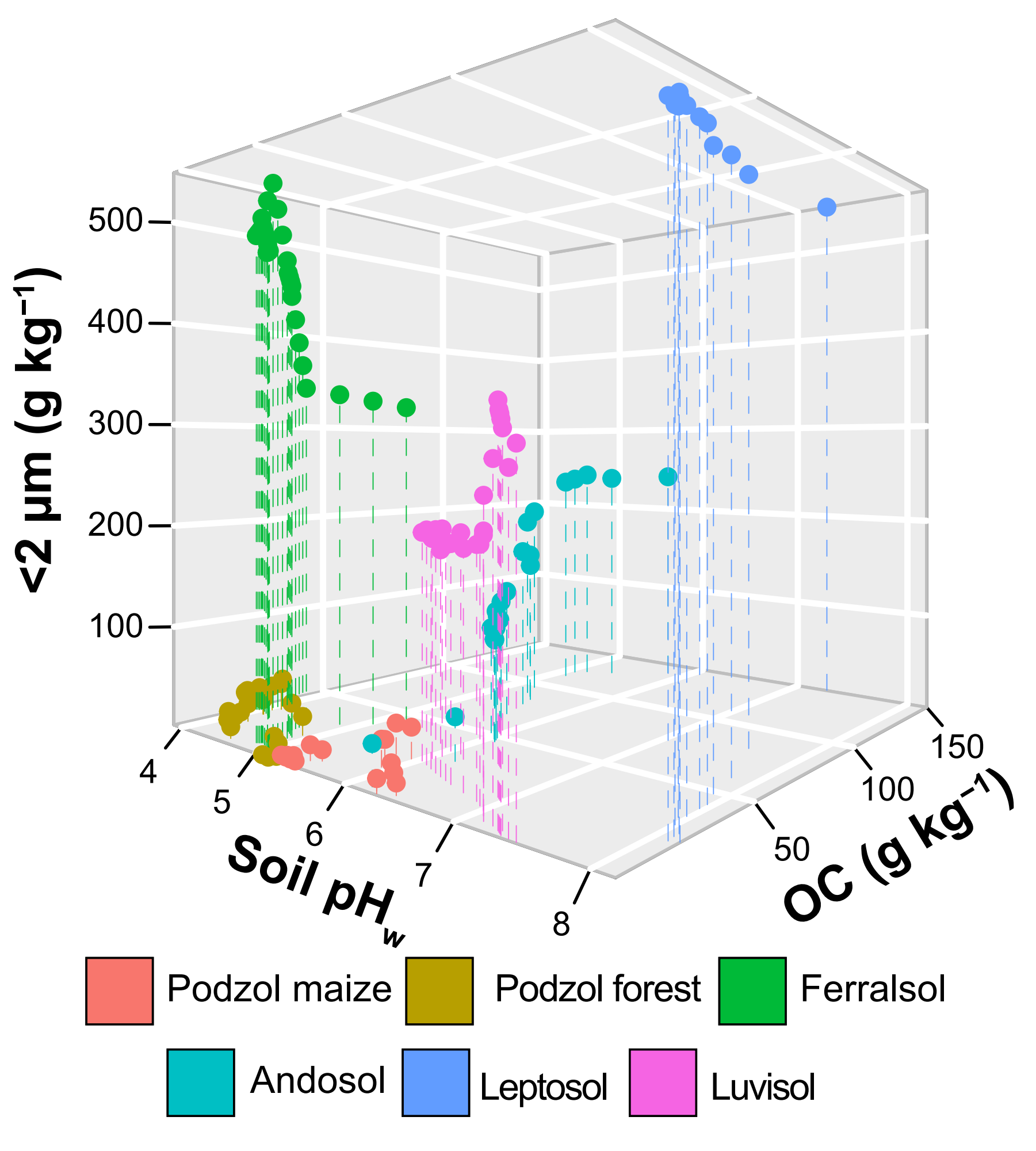
<2 µm (g kg⁻¹)
500
400
300
200
100
4
5
6
7
8
Soil pHw
150
100
50
OC (g kg⁻¹)
Podzol maize
Podzol forest
Ferralsol
Andosol
Leptosol
Luvisol

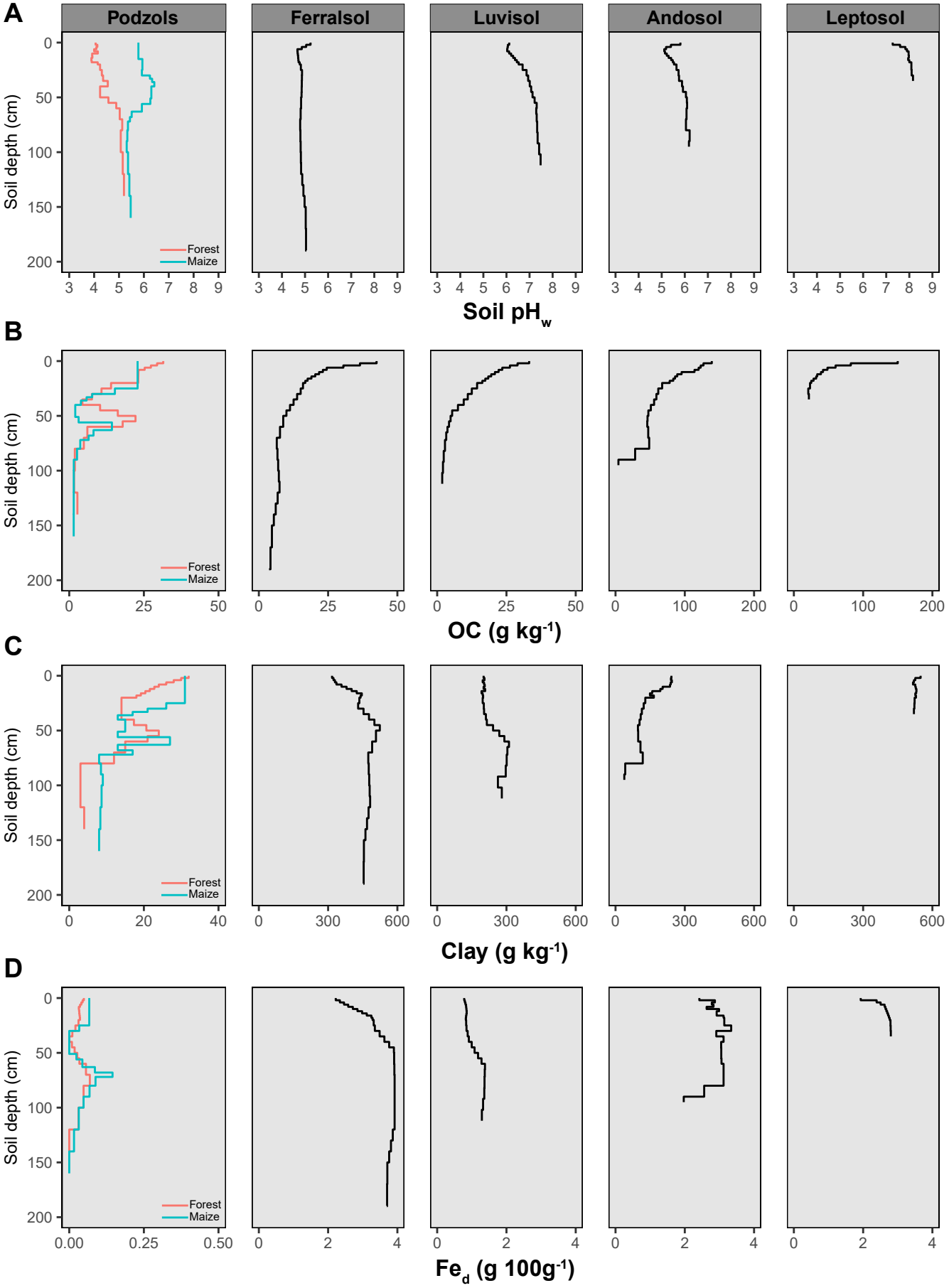
A
Podzols
Ferralsol
Luvisol
Andosol
Leptosol
Soil depth (cm)
0
50
100
150
200
Forest
Maize
3 4 5 6 7 8 9
Soil pH$_w$
B
Soil depth (cm)
Forest
Maize
0 25 50
0 100 200
OC (g kg^{-1})
C
Soil depth (cm)
Forest
Maize
0 20 40
0 300 600
Clay (g kg^{-1})
D
Soil depth (cm)
Forest
Maize
0.00 0.25 0.50
0 2 4
Fe$_d$ (g 100g^{-1})

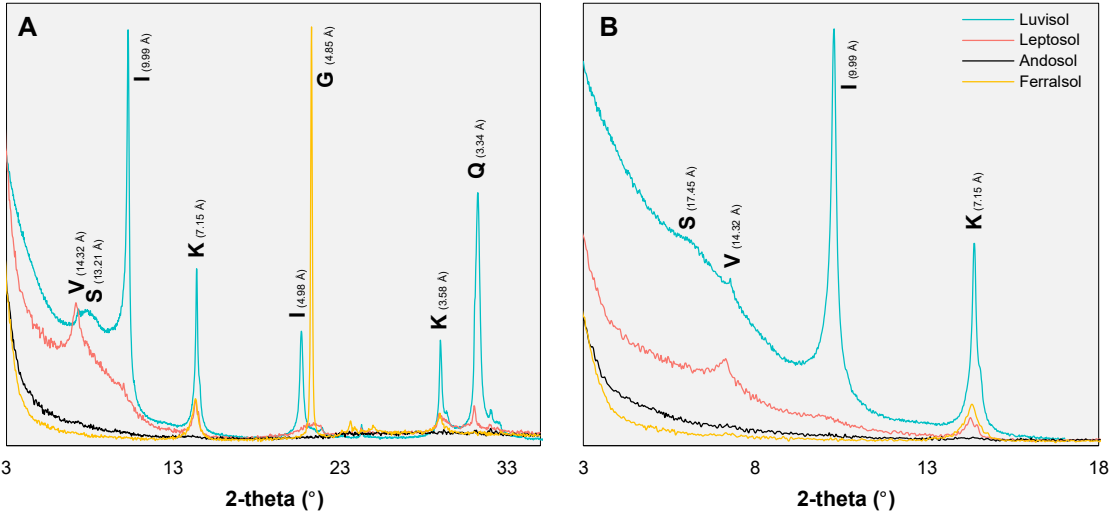
A
I (9.99 Å)
G (4.85 Å)
V (14.32 Å)
S (13.21 Å)
K (7.15 Å)
I (4.98 Å)
K (3.58 Å)
Q (3.34 Å)
3
13
23
33
2-theta (°)
B
Luvisol
Leptosol
Andosol
Ferralsol
I (9.99 Å)
S (17.45 Å)
V (14.32 Å)
K (7.15 Å)
3
8
13
18
2-theta (°)

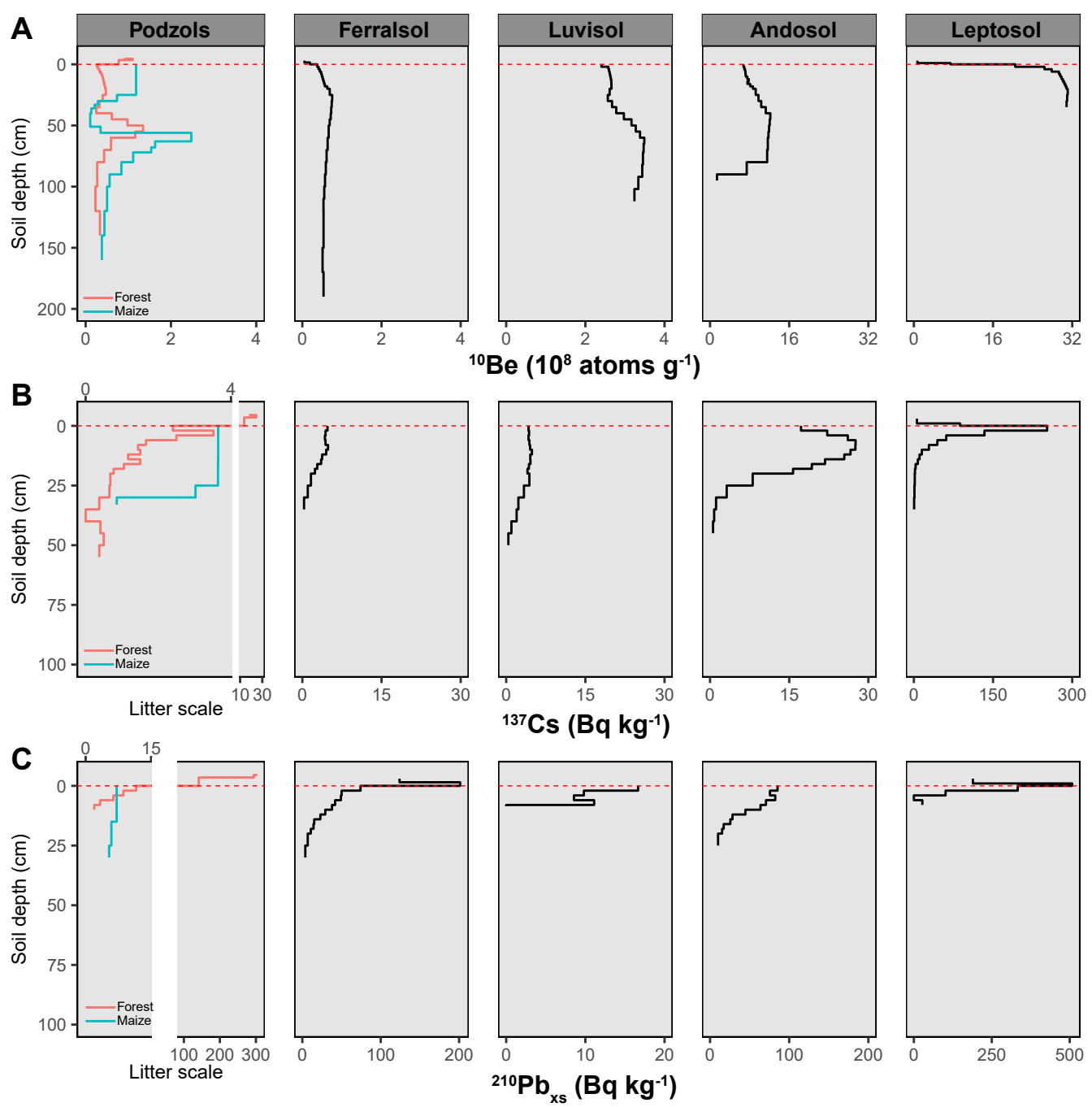
A
Podzols
Ferralsol
Luvisol
Andosol
Leptosol
Soil depth (cm)
Forest
Maize
^{10}Be (10^8 atoms g^{-1})
B
Litter scale
^{137}Cs (Bq kg^{-1})
C
^{210}Pb$_{xs}$ (Bq kg^{-1})

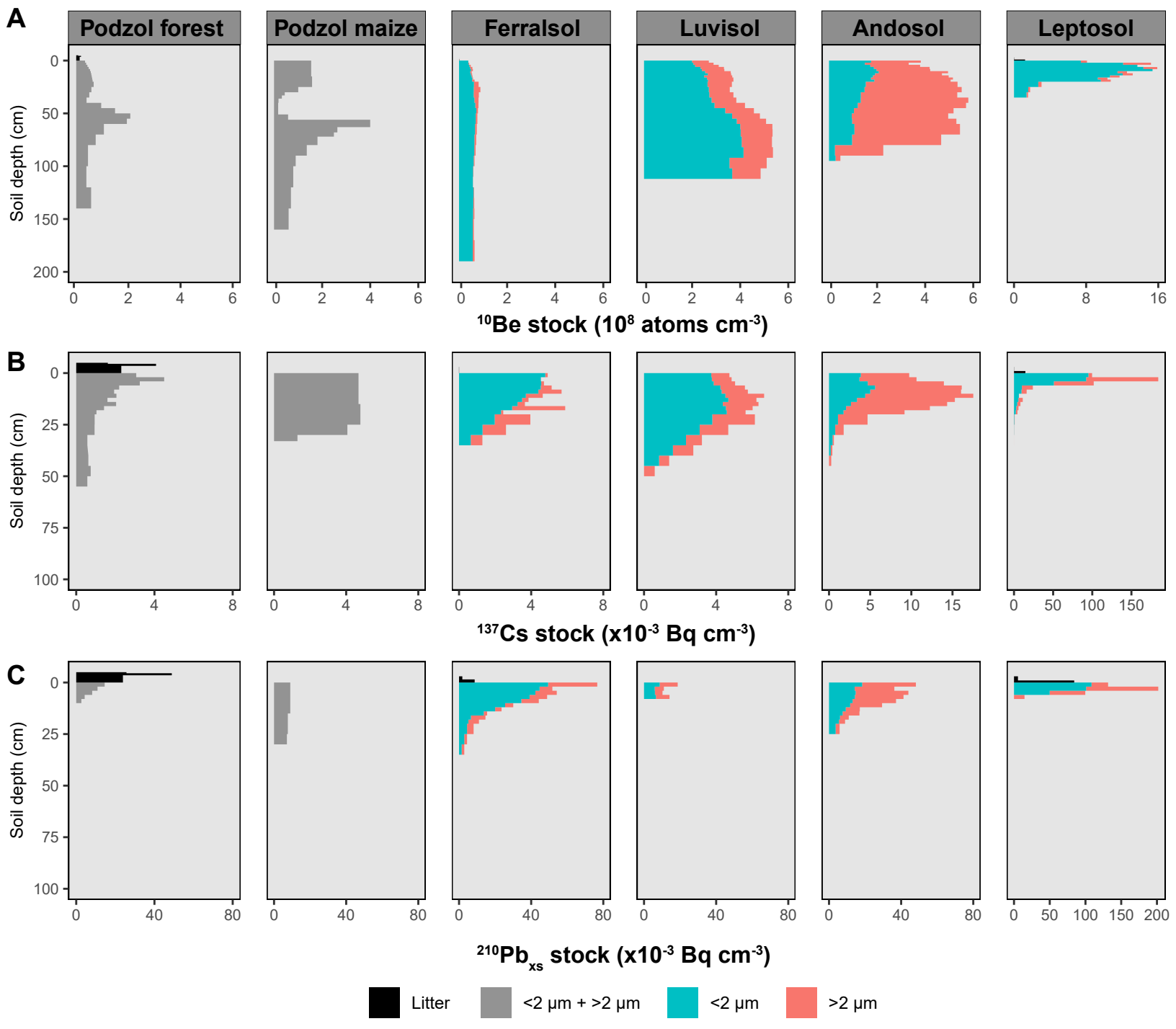
A
Podzol forest
Podzol maize
Ferralsol
Luvisol
Andosol
Leptosol
Soil depth (cm)
0
50
100
150
200
0 2 4 6
0 2 4 6
0 2 4 6
0 2 4 6
0 2 4 6
0 8 16
^{10}Be stock (10^8 atoms cm^{-3})
B
Soil depth (cm)
0
25
50
75
100
0 4 8
0 4 8
0 4 8
0 4 8
0 5 10 15
0 50 100 150
^{137}Cs stock (x10^{-3} Bq cm^{-3})
C
Soil depth (cm)
0
25
50
75
100
0 40 80
0 40 80
0 40 80
0 40 80
0 40 80
0 50 100 150 200
^{210}Pb$_{xs}$ stock (x10^{-3} Bq cm^{-3})
Litter
<2 µm + >2 µm
<2 µm
>2 µm

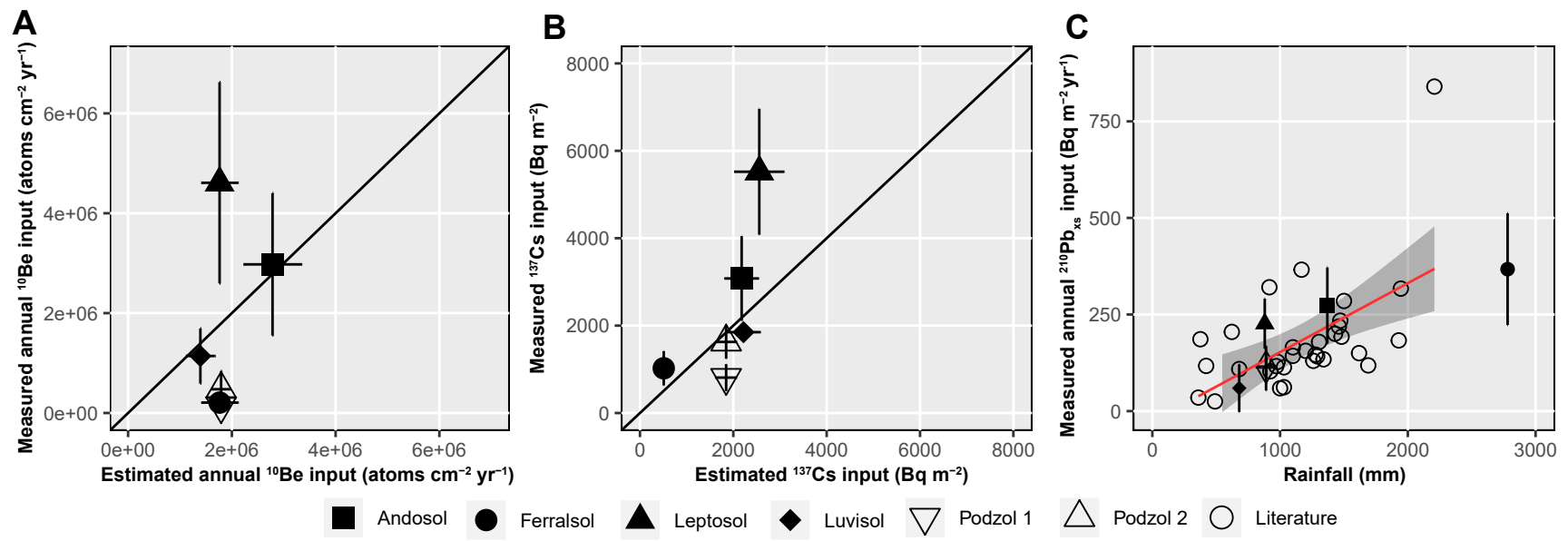
A
Measured annual ^{10}Be input (atoms cm^{-2} yr^{-1})
Estimated annual ^{10}Be input (atoms cm^{-2} yr^{-1})
0e+00
2e+06
4e+06
6e+06
B
Measured ^{137}Cs input (Bq m^{-2})
Estimated ^{137}Cs input (Bq m^{-2})
0
2000
4000
6000
8000
C
Measured annual ^{210}Pb$_{xs}$ input (Bq m^{-2} yr^{-1})
Rainfall (mm)
0
250
500
750
1000
2000
3000
Andosol
Ferralsol
Leptosol
Luvisol
Podzol 1
Podzol 2
Literature

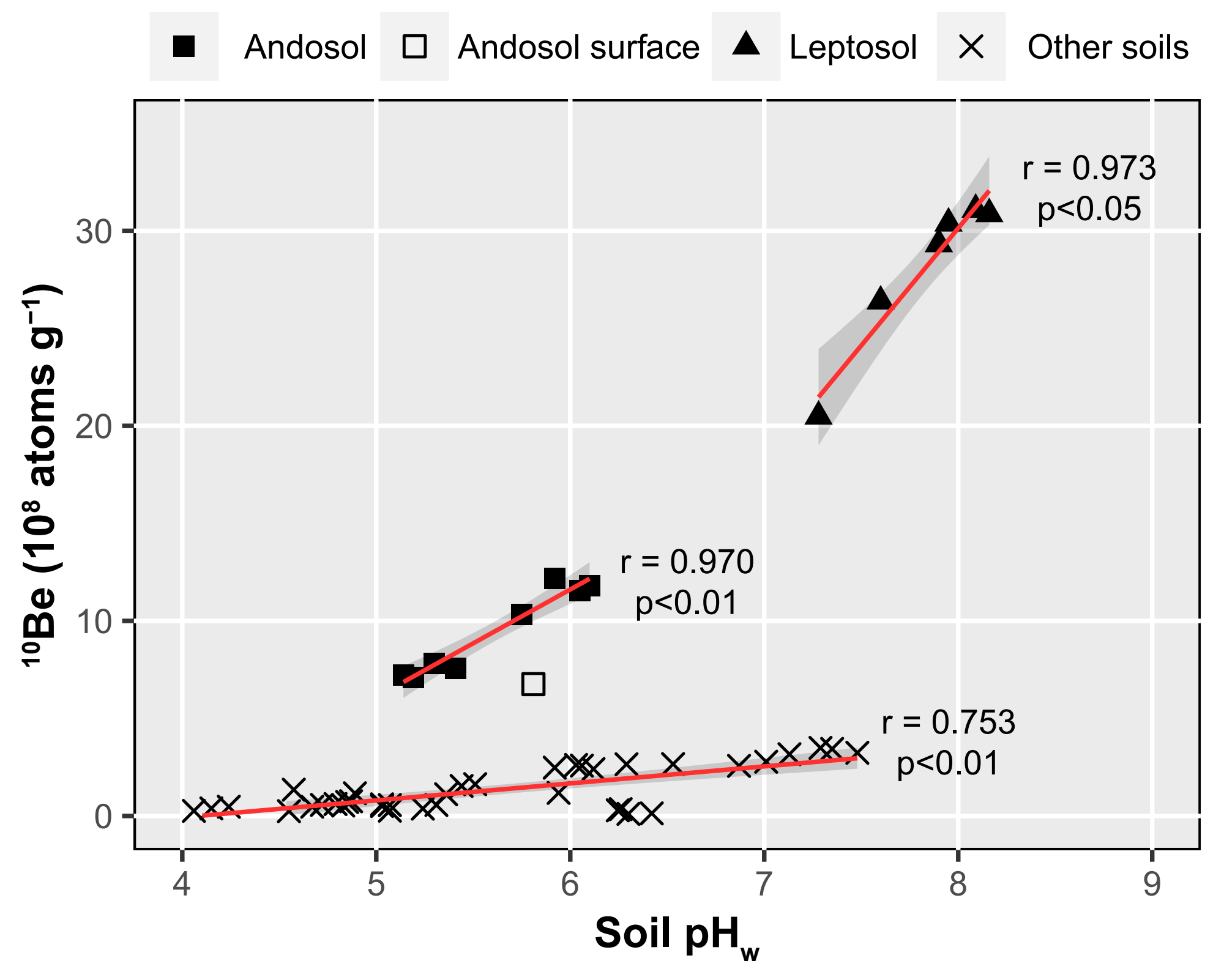
Andosol
Andosol surface
Leptosol
Other soils
r = 0.973
p<0.05
r = 0.970
p<0.01
r = 0.753
p<0.01
30
20
10
0
4
5
6
7
8
9
^{10}Be (10^8 atoms g^{-1})
Soil pH_w

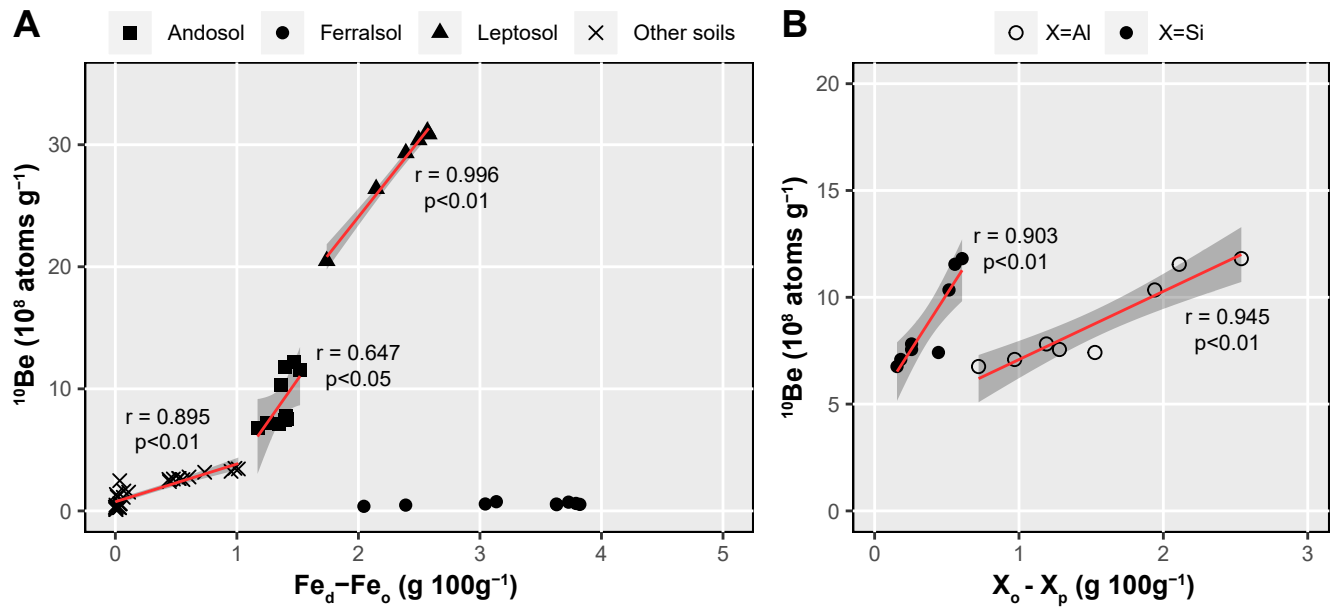
A
Andosol
Ferralsol
Leptosol
Other soils
r = 0.996
p<0.01
r = 0.647
p<0.05
r = 0.895
p<0.01
10Be (10^8 atoms g^-1)
Fe_d−Fe_o (g 100g^-1)
B
X=Al
X=Si
r = 0.903
p<0.01
r = 0.945
p<0.01
10Be (10^8 atoms g^-1)
X_o - X_p (g 100g^-1)

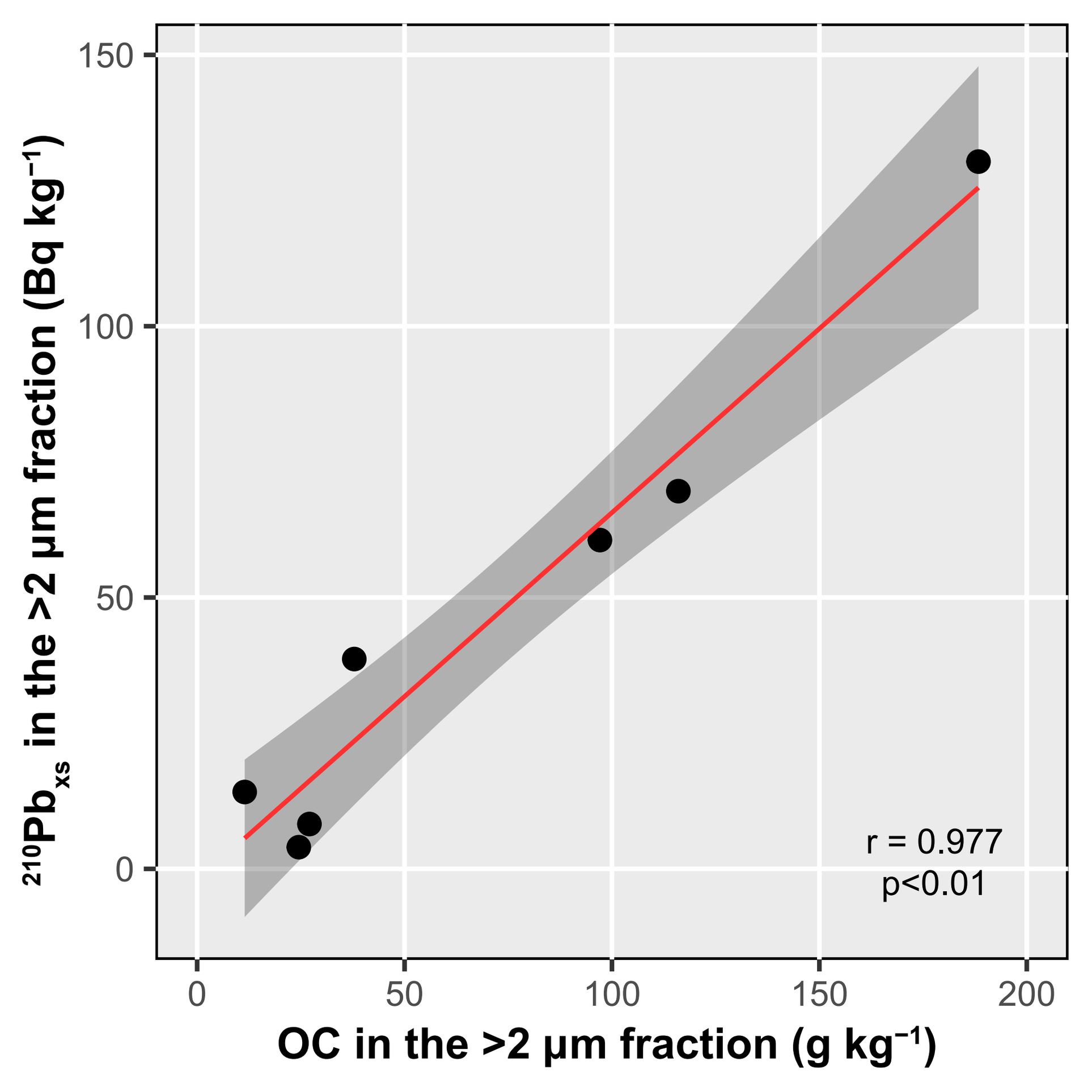
150
100
50
0
$^{210}Pb_{xs}$ in the >2 µm fraction (Bq kg^{-1})
r = 0.977
p<0.01
0
50
100
150
200
OC in the >2 µm fraction (g kg^{-1})

Table S1 – Bulk densities of the sampled soils.

Soil	Method	Sampling depth interval in cm	Bulk density (± SD)
Luvisol*	Gamma	0-5	1.10 ± 0.11
	Gamma	5-10	1.27 ± 0.04
	Gamma	10-15	1.37 ± 0.05
	Gamma	15-20	1.40 ± 0.04
	Gamma	20-25	1.40 ± 0.03
	Gamma	25-30	1.39 ± 0.03
	Gamma	30-35	1.39 ± 0.03
	Gamma	35-40	1.38 ± 0.04
	Cylinders	23-30	1.42 ± 0.05
	Cylinders	58-65	1.53 ± 0.03
	Cylinders	82-89	1.56 ± 0.03
	Cylinders	151-158	1.38 ± 0.05
Podzol 1	Cylinders	0-5	1.30 ± 0.12
	Cylinders	10-15	1.39 ± 0.02
	Cylinders	17-22	1.36 ± 0.06
	Cylinders	24-29	1.46 ± 0.02
	Cylinders	31-36	1.55 ± 0.02
	Cylinders	36-41	1.60 ± 0.02
	Cylinders	45-50	1.52 ± 0.04
	Cylinders	65-70	1.78 ± 0.18
	Cylinders	78-83	1.67 ± 0.02
	Cylinders	90-95	1.66 ± 0.03
	Cylinders	105-110	1.71 ± 0.03
Podzol 2	Cylinders	1-6	1.28 ± 0.05
	Cylinders	9-14	1.34 ± 0.01
	Cylinders	15-20	1.36 ± 0.03
	Cylinders	25-30	1.37 ± 0.03
	Cylinders	31-36	1.54 ± 0.01
	Cylinders	37-42	1.40 ± 0.01
	Cylinders	46-51	1.67 ± 0.02
	Cylinders	52-57	1.67 ± 0.02
	Cylinders	60-65	1.61 ± 0.03
	Cylinders	78-83	1.62 ± 0.06
	Cylinders	90-95	1.61 ± 0.05
	Cylinders	98-103	1.59 ± 0.01
Andosol	Cylinders	0-5	0.58 ± 0.07
	Cylinders	5-10	0.66 ± 0.03
	Cylinders	10-15	0.72 ± 0.05
	Cylinders	15-20	0.77 ± 0.04
	Cylinders	20-25	0.80 ± 0.06
	Cylinders	25-30	0.79 ± 0.07
	Cylinders	30-35	0.75 ± 0.06
	Cylinders	42-47	0.75 ± 0.07
	Cylinders	55-60	0.94 ± 0.29
	Cylinders	67-72	0.97 ± 0.35
	Cylinders	76-81	0.89 ± 0.01
Ferralsol	Excavation-water method	0-5	1.02 ± 0.06
	Excavation-water method	5-10	1.24 ± 0.01
	Cylinders	11-20	1.03 ± 0.12
	Cylinders	21-30	1.18 ± 0.04
	Cylinders	31-40	1.11 ± 0.02
	Cylinders	43-52	1.14 ± 0.02
	Cylinders	54-63	1.14 ± 0.06
	Cylinders	68-77	1.16 ± 0.01
	Cylinders	80-89	1.16 ± 0.06
	Cylinders	106-115	1.08 ± 0.02
	Cylinders	120-129	1.17 ± 0.04
	Cylinders	155-164	1.20 ± 0.04

*according to Jagercikova et al. (2015)

Table S2 – Soil physicochemical characteristics (3 pages)

Soil	Depth	Stones + rock content	<2 µm	2-20 µm	20-50 µm	50-200 µm	200-2000 µm	pH_w	$CaCO_3$	OC	HF	Pyrophosphate			Dithionite			Oxalate		
											Fe	Fe	Si	Al	Fe	Si	Al	Fe	Si	Al
	cm	%	g kg^{-1}						g kg^{-1}		g $100g^{-1}$									
Luvisol*	0 - 2		201	300	444	47	8	6.12		33.2	2.06				0.78			0.34		
	2 - 4		205	302	436	47	10	6.06		29.0	2.09				0.80			0.36		
	4 - 6		197	313	431	46	13													
	6 - 8		203	293	449	45	10	6.03		23.5	2.19				0.83			0.36		
	8 - 10		206	306	432	44	12													
	10 - 12		201	313	427	42	17													
	12 - 14		208	299	436	44	13	6.29		19.5	2.24				0.85			0.33		
	14 - 16		192	319	417	59	13													
	16 - 18		197	310	420	59	14													
	18 - 20		199	296	449	47	9	6.53		16.3	2.24				0.83			0.31		
	20 - 25		197	316	424	54	9													
	25 - 30		202	296	447	46	9	6.87		12.5	2.22				0.85			0.29		
	30 - 35		203	309	429	48	11													
	35 - 40		211	301	439	38	11	7.01		9.6	2.27				0.91			0.31		
	40 - 45		215	312	414	50	9													
	45 - 50		242	309	402	42	5	7.13		5.4	2.61				1.08			0.35		
	50 - 55		269	323	360	43	5													
	55 - 60		291	322	339	42	6	7.31												
	60 - 65		311	301	352	33	3	7.29		3.7	3.37				1.38			0.40		
	65 - 72		304	296	354	43	3													
	72 - 82		301	279	373	44	3													
	82 - 92		297	277	390	34	2	7.35		2.4	3.30				1.36			0.35		
	92 - 102		263	284	400	50	3													
	102 - 112		280	261	422	35	2	7.48		1.8	3.16				1.29			0.34		
	112 - 122		251	209	481	55	4													
	122 - 132		235	196	527	40	2	7.53		1.7	2.67				1.14			0.26		
	132 - 142		210	216	542	28	3		<1											
	142 - 152		183	232	568	16	1	7.56		1.3	2.49				1.07			0.26		
	152 - 162		197	277	506	17	2		<1											
Podzol 1	0 - 2		32	13	5	42	908	4.06		31.5	0.07	0.01	0.03	0.02	0.05			0.02		
	2 - 4							4.13												
	4 - 6							4.09												
	6 - 8							4.00												
	8 - 10		24	12	5	30	929	4.15		23.2	0.07	0.03	0.04	0.04	0.03			0.03		
	10 - 12							3.92												
	12 - 14							3.93												
	14 - 16							3.89												
	16 - 18							3.90												
	18 - 20		18	11	2	37	932	4.15		23.1	0.08				0.04			0.03		

Podzol 1	20 - 25		14	2	1	16	967	4.24		14.0	0.08	0.03	0.02	0.06	0.03			0.03	
	25 - 30							4.31											
	30 - 35							4.36											
	35 - 40		14	2	5	26	953	4.55		4.4	0.05	0.01	0.03	0.02	<0.02			<0.008	
	40 - 45							4.24											
	45 - 50							4.24											
	50 - 55		24	1	1	47	927	4.58		22.2	0.08	0.02	0.09	0.23	0.03			0.02	
	55 - 60		21	3	2	59	915	4.89		17.9	0.09	0.02	0.10	0.36	0.03			0.02	
	60 - 70		15	5	2	53	925	5.03		6.1	0.15	0.03	0.31	0.25	0.06			0.02	
	70 - 80		12	5	1	25	957	5.13		4.9	0.19				0.07			0.02	
	80 - 100		3	4	1	47	945	5.07		1.9	0.16	0.01	0.11	0.11	0.05			0.01	
	100 - 120		3	1	2	22	972	5.15		1.6	0.16	0.01	0.10	0.11	0.03			0.01	
	120 - 140		4	5	1	15	975	5.20		2.7	0.09	0.01	0.13	0.10	<0.02			<0.008	
Podzol 2	0 - 15							5.78											
	15 - 25		31	15	4	39	911	5.94		22.9	0.14	0.04	0.06	0.09	0.07			0.05	
	25 - 30							5.92											
	31 - 33		21	3	9	49	918	6.25		7.7	0.07	0.01	0.03	0.03	<0.02			0.02	
	36 - 40		13	9	2	30	946	6.42		3.9	0.06	0.01	0.03	0.01	<0.02			0.01	
	40 - 51		15	2	2	35	946	6.30		2.0	0.06	0.01	0.05	0.01	<0.02			<0.008	
	51 - 56		13	2	2	53	930	6.26		3.1	0.07	0.01	0.05	0.03	0.02			<0.008	
	56 - 63		27	2	1	42	928	5.92		14.3	0.14	0.02	0.17	0.28	0.04			0.01	
	63 - 68		13	5	1	30	951	5.51		8.1	0.18	0.04	0.22	0.26	0.09			0.02	
	68 - 72		17	2	1	32	948	5.44		6.5	0.23	0.07	0.15	0.27	0.15			0.04	
	72 - 80		8	4	3	15	970	5.36		3.7	0.17	0.04	0.19	0.18	0.09			0.02	
	90 - 100		9	2	2	12	975	5.31		1.5	0.11	0.02	0.10	0.10	0.05			0.01	
	140 - 160		8	1	1	18	972	5.47		1.5	0.08				<0.02			<0.008	
Leptosol	0 - 2	15.4	549	210	126	93	19	7.28	3	150.0	2.97				1.93			0.19	
	2 - 4	25.9	526	202	132	101	29	7.60	9	82.2	3.78				2.39			0.24	
	4 - 6	36.4	520	202	138	104	23	7.83	12	60.2									
	6 - 8	45.0	516	198	137	100	36	7.90	12	48.5	4.15				2.62			0.23	
	8 - 10	45.0	526	198	142	99	32	7.97	3	42.1									
	10 - 12	60.1	528	199	137	102	28	7.97	6	39.1									
	12 - 14	60.1	531	196	141	102	23	7.98	7	33.7									
	14 - 16	65.2	530	193	133	103	32	7.95	9	32.2	4.28				2.72			0.22	
	16 - 18	70.3	526	198	135	104	31	8.00	6	28.4									
	18 - 20	70.3	529	191	141	105	26	8.09	8	25.1									
	20 - 25	91.8	523	190	145	114	23	8.09	5	23.3	4.35				2.79			0.22	
	25 - 30	95.3	522	195	136	111	27	8.10	9	20.8									
	30 - 35	95.8	520	192	142	110	27	8.16	9	21.7	4.31				2.80			0.22	
Andosol	0 - 2	0.0	242	400	116	61	181	5.81		139.0	4.96	0.78	0.35	1.30	2.42	0.52	1.74	1.25	0.50	2.02
	2 - 4	4.2	240	438	92	62	168	5.40		127.0	5.21	0.93	0.43	1.57	2.87	0.52	2.22	1.41	0.51	2.51
	4 - 6	3.3	244	451	90	70	145	5.19		123.0	5.15	0.84	0.31	1.39	2.78	0.49	2.13	1.43	0.49	2.36
	6 - 8	2.7	239	467	97	67	130	5.11		120.0	5.30	0.92	0.41	1.57	2.83	0.50	2.24	1.41	0.49	2.56
	8 - 10	2.8	236	458	106	70	130	5.14		114.0	5.18				2.63	0.52	2.03	1.38	0.50	2.39
	10 - 12	5.9	204	460	106	77	153	5.22		95.4	5.55	1.01	0.48	1.73	2.99	0.52	2.39	1.47	0.53	2.73
	12 - 14	8.7	194	454	112	75	165	5.30		89.1	5.74	0.84	0.29	1.40	2.92	0.49	2.29	1.52	0.55	2.59

Andosol	14 - 16	4.8	159	418	97	65	261	5.41	86.0	5.80	0.81	0.29	1.39	2.92	0.52	2.28	1.51	0.55	2.67
	16 - 18	4.8	149	413	97	76	265	5.48	83.4	6.18	0.85	0.35	1.49	3.12	0.52	2.44	1.42	0.54	2.68
	18 - 20	7.4	166	457	103	88	186	5.53	78.2	6.20	0.81	0.33	1.40	3.14	0.56	2.50	1.46	0.59	2.59
	20 - 25	12.9	129	458	102	76	235	5.64	67.3	6.31	0.78	0.32	1.33	3.14	0.57	2.54	1.41	0.62	2.95
	25 - 30	9.8	122	466	121	85	206	5.73	61.7	6.63	0.82	0.30	1.30	3.34	0.55	2.66	1.46	0.64	2.96
	30 - 35	8.7	114	484	134	88	180	5.75	59.0	6.44	0.76	0.18	1.18	2.91	0.43	2.18	1.55	0.70	3.12
	37 - 40	8.9	109	479	140	92	180	5.88	55.7	6.66	0.91	0.22	1.24	3.12	0.42	2.32	1.57	0.73	3.21
	40 - 45	21.8	104	478	133	83	202	5.92	51.0	7.10				3.05	0.43	2.13	1.58	0.77	3.17
	45 - 50	23.6	97	470	149	85	199	6.05	47.4										
	50 - 55	24.2	98	463	135	96	208	6.09	46.2										
	55 - 60	22.6	98	471	147	95	189	6.10	45.8	6.73	0.76	0.18	1.10	3.06	0.42	2.17	1.67	0.79	3.64
	60 -70	21.4																	
	70 - 80	24.1	118	488	127	89	178	6.05	48.6	6.95	0.83	0.22	1.14	3.12	0.40	2.04	1.60	0.78	3.25
	80 - 90	28.9	42	359	152	62	385	6.21	28.3	7.05	0.49	0.13	0.72	2.56	0.32	1.49	1.16	0.57	2.25
	90 - 95	27.3	38	326	137	100	399	6.18	4.2	6.85	0.09	0.12	0.29	1.97	0.32	0.72	0.54	0.28	0.97
Ferralsol	0 - 2		317	50	17	64	552	5.24	42.5	2.61				2.22			0.18		
	6 - 8		336	45	19	68	532	4.67	24.5	3.01				2.58			0.19		
	16 - 18		446	52	20	78	404	4.72	17.6	3.85				3.25			0.21		
	25 - 30		430	53	19	68	430	4.87	15.1	4.09				3.35			0.22		
	45 - 50		524	49	17	70	340	4.85	10.0	4.94				3.90			0.17		
	70 - 80		474	41	20	62	403	4.79	6.5	5.13				3.92			0.13		
	110 - 120		482	43	21	60	394	4.83	7.5	5.16				3.92			0.10		
	150 - 170		455	60	5	53	427	5.03	4.7	4.88				3.71			0.08		
	210 - 230		452	48	6	55	439	5.07	3.2	4.82				3.69			0.06		

*according to Jagercikova et al. (2014b, 2015) for particle-size distribution, OC concentration and pH. The other analyses are derived from the current study.

Table S3 - Isotope concentrations in the studied bulk soils (2 pages)

Soil	Depth in cm	^{137}Cs (Bq kg^{-1})	^{210}Pb$_{(xs)}$ (Bq kg^{-1})	meteoric ^{10}Be (10^8 atoms g^{-1})
Luvisol*	0 - 2	4.23 ± 0.19	16.66 ± 1.87	2.41 ± 0.08
	2 - 4	4.34 ± 0.18	9.82 ± 1.73	2.58 ± 0.08
	4 - 6	4.22 ± 0.19	8.56 ± 1.80	nd
	6 - 8	4.40 ± 0.19	11.11 ± 1.76	2.61 ± 0.10
	8 - 10	4.53 ± 0.19	< 4.15	nd
	10 - 12	4.88 ± 0.17	< 3.23	nd
	12 - 14	4.56 ± 0.19	6.12 ± 1.71	2.65 ± 0.10
	14 - 16	4.59 ± 0.21	< 4.45	nd
	16 - 18	4.31 ± 0.20	5.85 ± 2.17	nd
	18 - 20	4.03 ± 0.17	4.90 ± 1.62	2.66 ± 0.10
	20 - 25	4.40 ± 0.20	< 4.25	nd
	25 - 30	3.36 ± 0.16	< 3.04	2.57 ± 0.10
	30 - 35	2.31 ± 0.10	< 2.12	nd
	35 - 40	1.98 ± 0.13	< 2.86	2.78 ± 0.11
	40 - 45	0.99 ± 0.15	< 4.24	nd
	45 - 50	0.41 ± 0.08	< 1.95	3.17 ± 0.09
	50 - 55	< 0.25	< 3.80	nd
	55- 60	< 0.24	< 3.92	nd
	60 - 65	< 0.23	< 3.11	3.49 ± 0.10
	82 - 92	< 0.22	< 2.96	3.44 ± 0.15
	102 - 112	< 0.22	< 2.86	3.24 ± 0.09
	122 - 132	< 0.22	< 3.03	3.02 ± 0.10
Podzol 1	OL (Litter)	18.92 ± 0.82	300.84 ± 8.70	0.91 ± 0.01
	OF (Litter)	24.52 ± 0.69	293.63 ± 6.39	1.10 ± 0.02
	OH (Litter)	13.63 ± 0.37	141.28 ± 3.34	0.78 ± 0.01
	0 - 2	2.36 ± 0.11	11.18 ± 0.93	0.26 ± 0.01
	2 - 4	3.46 ± 0.14	8.38 ± 1.01	nd
	4 - 6	2.46 ± 0.12	6.16 ± 0.92	nd
	6 - 8	1.63 ± 0.11	3.21 ± 0.92	nd
	8 - 10	1.42 ± 0.09	1.92 ± 0.74	0.39 ± 0.01
	10 - 12	1.48 ± 0.09	< 1.60	nd
	12 - 14	1.15 ± 0.06	< 1.11	nd
	14 - 16	1.48 ± 0.11	< 1.59	nd
	16 - 18	1.04 ± 0.06	< 1.15	nd
	18 - 20	0.76 ± 0.07	< 1.58	nd
	20 - 25	0.67 ± 0.08	< 1.65	0.47 ± 0.01
	25 - 30	0.64 ± 0.08	< 1.66	nd
	30 - 35	0.37 ± 0.05	< 1.18	nd
	35 - 40	< 0.20	< 1.80	0.25 ± 0.01
	40 - 45	0.40 ± 0.08	< 1.63	nd
	45 - 50	0.49 ± 0.06	< 1.27	nd
	50 - 55	0.37 ± 0.05	< 1.10	1.35 ± 0.02
	55 - 60	< 0.22	< 1.79	1.16 ± 0.02
	60 - 70	nd	nd	0.59 ± 0.02
	70 - 80	< 0.16	< 1.28	nd
	80 - 100	nd	nd	0.27 ± 0.01
Podzol 2	0 - 15	3.59 ± 0.09	6.88 ± 0.66	nd
	15 - 25	3.58 ± 0.14	5.71 ± 0.98	1.18 ± 0.03
	25 - 30	2.97 ± 0.11	5.21 ± 0.83	nd
	31 - 33	0.84 ± 0.09	< 1.85	0.29 ± 0.01
	33 - 36	< 0.24	< 1.60	nd
	36 - 40	nd	nd	0.13 ± 0.01
	40 - 51	< 0.18	< 1.66	0.11 ± 0.01
	51 - 56	< 0.18	< 1.76	0.35 ± 0.01
	56 - 63	nd	nd	2.48 ± 0.05
	64 - 68	nd	nd	1.63 ± 0.03
	68 - 72	< 0.12	< 1.73	1.54 ± 0.04
	72 - 80	nd	nd	1.11 ± 0.03
	90 - 100	nd	nd	0.56 ± 0.02
Leptosol	Vegetation	nd	nd	0.16 ± 0.00
	OL (Litter)	5.77 ± 0.42	189.34 ± 4.52	0.72 ± 0.01
	OF (Litter)	87.59 ± 1.65	507.90 ± 10.02	7.40 ± 0.12
	0 - 2	252.46 ± 1.66	333.18 ± 5.71	20.48 ± 0.28
	2 - 4	133.77 ± 0.80	101.65 ± 2.96	26.39 ± 0.12
	4 - 6	61.35 ± 0.64	< 5.75	nd
	6 - 8	44.51 ± 0.49	27.14 ± 2.53	29.32 ± 0.41

Leptosol	8 - 10	28.48 ± 0.45	< 5.35	nd
	10 - 12	15.06 ± 0.21	< 3.08	nd
	12 - 14	10.79 ± 0.30	< 5.01	nd
	14 - 16	7.48 ± 0.28	< 5.65	30.38 ± 0.43
	16 - 18	3.29 ± 0.21	< 5.07	nd
	18 - 20	2.09 ± 0.13	< 3.15	nd
	20 - 25	1.69 ± 0.12	< 3.18	31.09 ± 0.12
	25 - 30	1.11 ± 0.14	< 4.03	nd
	30 - 35	0.50 ± 0.14	< 3.86	30.86 ± 0.43
	Parent rock	nd	nd	0.11 ± 0.00
Andosol	Roots (0 - 2 cm)	6.85 ± 0.65	70.42 ± 6.48	nd
	0 - 2	17.24 ± 0.36	85.27 ± 2.93	6.76 ± 0.12
	2 - 4	22.20 ± 0.44	75.69 ± 3.02	nd
	4 - 6	26.11 ± 0.53	82.36 ± 3.56	7.09 ± 0.14
	6 - 8	27.58 ± 0.52	70.66 ± 3.29	nd
	8 - 10	27.54 ± 0.55	63.80 ± 3.45	7.23 ± 0.12
	10 - 12	26.62 ± 0.46	44.70 ± 2.74	nd
	12 - 14	25.43 ± 0.50	28.41 ± 3.06	7.82 ± 0.17
	14 - 16	21.79 ± 0.49	25.63 ± 3.28	7.56 ± 0.12
	16 - 18	19.29 ± 0.44	17.24 ± 3.02	nd
	18 - 20	15.73 ± 0.38	15.23 ± 2.73	nd
	20 - 25	8.08 ± 0.19	10.13 ± 1.62	nd
	25 - 30	3.16 ± 0.20	< 4.60	nd
	30 - 35	1.14 ± 0.19	< 4.89	10.34 ± 0.17
	37 - 40	0.78 ± 0.11	5.26 ± 1.60	nd
	40 - 45	0.57 ± 0.13	< 4.26	12.18 ± 0.19
	45 - 50	< 0.30	< 3.26	nd
	50 - 55	< 0.55	5.58 ± 2.51	nd
	55 - 60	< 0.34	< 3.26	11.81 ± 0.20
	70 - 80	< 0.34	3.59 ± 1.60	11.55 ± 0.20
	80 - 90	nd	nd	7.42 ± 0.03
	Parent rock	nd	nd	0.70 ± 0.02
Ferralsol	OL1	< 1.77	124.00 ± 7.01	0.05 ± 0.00
	OL2	< 1.37	201.28 ± 6.41	0.19 ± 0.01
	0 - 2	4.76 ± 0.17	74.19 ± 1.75	0.38 ± 0.02
	2 - 4	4.40 ± 0.18	50.08 ± 1.76	nd
	4 - 6	4.28 ± 0.19	49.21 ± 1.84	nd
	6 - 8	4.39 ± 0.20	41.78 ± 1.87	0.47 ± 0.02
	8 - 10	4.86 ± 0.20	37.83 ± 1.85	nd
	10 - 12	4.52 ± 0.12	29.27 ± 1.09	nd
	12 - 14	3.75 ± 0.20	22.95 ± 1.75	nd
	14 - 16	3.56 ± 0.19	15.15 ± 1.80	nd
	16 - 18	2.82 ± 0.13	14.27 ± 1.28	0.57 ± 0.02
	18 - 20	2.39 ± 0.16	10.75 ± 1.56	nd
	20 - 25	1.63 ± 0.10	6.85 ± 1.01	nd
	25 - 30	1.02 ± 0.12	3.76 ± 1.40	0.75 ± 0.03
	30 - 35	0.32 ± 0.08	< 2.13	nd
	35 - 40	< 0.30	< 1.17	nd
	40 - 45	nd	nd	0.72 ± 0.02
	70 - 80	nd	nd	0.61 ± 0.03
	110 - 120	nd	nd	0.53 ± 0.02
	150 - 170	nd	nd	0.51 ± 0.02
	210 - 230	nd	nd	0.56 ± 0.02

*according to Jagercikova et al. (2014b, 2015)